Impact of Allee effect in Leslie-Gower model with increasing functional response

Predrag Z. Djordjević[a,*], Jelena V. Manojlović[b]

[a]*Mathematical Institute of the Serbian Academy of Sciences and Arts*
[b]*University of Nis, Faculty of Science and Mathematics, Department of Mathematics*

Abstract. This paper presents a study of dynamic behavior and bifurcation analysis of a predator–prey system with the functional response proposed by Cosner et al. (Theor Popul Biol 56:65–75, 1999) and Allee effect in prey population. The functional response used is specific in compare with the conventional functional responses according to its monotonicity for both prey and predator density, and moreover it increases as predator density increase. This function response describes a behavioral mechanism which a group of predators foraging in linear formation, contacts and then hunts gathering around the herd or a school of prey. Mainly, our aim is to demonstrate the impact of strong and weak Allee effect on the system dynamics. Mathematically our analysis primarily focuses on the stability of coexisting equilibrium points and all possible bifurcations that the system may exhibit. Actually, we consider the existence of equilibria and analyze their stability. The possibility of extinction of both populations is also considered, by studying dynamics of the system near the origin. The bifurcation of the system will be analyzed, including the occurrence of saddle–node bifurcation, Hopf and degenerate Hopf bifurcation, and Bogdanov–Takens bifurcation. The theoretical results are verified by numerical simulations. We observe the bi-stability and tri-stability, so that we further discuss the basins of attraction in all possible cases of existence of multiple attractors.

1. Introduction

Population biology is a subfield of biology that focuses on the study how populations interact with one another, including competition, predation, and symbiosis, and how these interactions shape the evolution of populations over time. Often such studies are vital to decisions made about how to protect endangered species. Mathematical models play a key part in simulation of the growth and behavior of populations under different environmental conditions, as well as to investigate the effects of factors such as predation, competition, disease, and climate change on population dynamics. The predator-prey model is a type of mathematical model that is commonly used in population biology to study the dynamics of predator and

prey populations in an ecosystem. The complexity of the model depends solely on the species that are being observed and behaviour tactics they employ in order to survive. Classic predator-prey models are given with

$$\dot{x} = xf(x) - p(x, y)y$$
$$\dot{y} = g(p(x, y), y)y$$

where variables x and y describe densities of predator and prey, respectively. Function $f(x)$ is the per capita prey growth rate in the absence of predators, while $g(p(x, y), y)$ is predator growth function. The most often used example of prey growth rate is the logistic form $f(x) = r(1 - x/k)$, where the positive constants r and k refer to the intrinsic growth rate of prey and the carrying capacity of the environment for the prey population, respectively. The functional response of a predator describes the relationship between the number of prey it consumes per unit of time and the abundance or density of its prey.

Considering $g(p(x, y), y) = cp(x, y) - \mu y$ we get the following model [8]:

$$\dot{x} = rx\left(1 - \frac{x}{k}\right) - p(x, y)y$$
$$\dot{y} = cp(x, y) - \mu y,$$
(1)

where, c is the biomass conversion rate while μ is the death rate of predators.

Leslie and Gower [17] proposed a predator-prey model, the so-called Leslie-Gower predator-prey model, in which the predator growth function is different from the predator predation function. They assumed that the predator growth is described by a function of the ratio of predators and their prey. Leslie–Gower type models are characterized by a logistic-type predator growth equation, where the environmental carrying capacity of predators k_y is a function of the available prey quantity [28], that is, $k_y = k(x) = nx$. Leslie-Gower predator-prey models are given by:

$$\dot{x} = rx\left(1 - \frac{x}{k}\right) - p(x, y)y$$
$$\dot{y} = sy\left(1 - \frac{y}{nx}\right)$$
(2)

where s is intrinsic growth rate of predators and n measures the food quality of the prey for conversion into predator units. In this type of models, the predator population growth rate depends on the predator population size ratio to the prey population size and a positive growth rate is predicted when the absolute prey and predator densities are significantly low. Term $\frac{y}{nx}$ is called Leslie-Gower term. In order to consider different behavioral characteristics of species in mutual relations different forms of functional response were introduced. Throughout years different functional responses were observed:

(i) Holling-type I or Lotka-Volterra type, $p(x, y) = h(x) = px$;

(ii) Holling-type II, $p(x, y) = h(x) = \frac{px}{x+a}$;

(iii) Holling-type III, $p(x, y) = h(x) = \frac{px^2}{x^2+b}$ or generalized Holling-type III $p(x, y) = h(x) = \frac{px^2}{ax^2+bx+1}$;

(iv) Holling-type IV, $p(x, y) = h(x) = \frac{px}{x^2+b}$ or generalized Holling-type IV, $p(x, y) = h(x) = \frac{px}{ax^2+bx+1}$;

(v) Ivlev-type, $p(x, y) = h(x) = p(1 - e^{-ax})$.

(vi) Beddington-DeAngelis, $p(x, y) = \frac{px}{ax+by+c}$;

(vii) Hassell-Varley-Holling II, $p(x, y) = \frac{px}{ax+y^{\gamma}}, \gamma \in (0, 1)$;

(viii) Ratio-Dependant Holling-type II, $p(x, y) = h\left(\frac{y}{x}\right) = \frac{px}{x+ay}$;

(ix) Ratio-Dependant Holling-type III, $p(x, y) = h\left(\frac{y}{x}\right) = \frac{px^2}{x^2 + ay^2}$;

Constants a, b, c and p used above are positive, and they have appropriate biological meanings in each response function (see [31] for (i), [3, 12] for (ii), [16, 20] for (iii), [24, 33] for (iv), [13] for (v), [32] for (vi), [29] for (vii), [15] for (viii), [18] for (ix)). Functional responses (i)-(v) are prey dependent functional responses, while (vi) and (vii) are predator and prey dependent functional responses, (viii), (ix) fall into a class of ratio-dependent functional responses. It is also important to note that functional responses (i)-(iii) and (v)-(ix) are monotonic, meaning that they are either non-increasing or non-decreasing with respect to either x or y. On the other hand, functional responses (iv) are non-monotonic, since they are increasing until they reach the maximum for x^*, after which they are decreasing.

In order to better describe the predator-prey interactions additional natural phenomena can be incorporated into mathematical models. One of those phenomena is hunting cooperation. It is one of many strategies that predator population utilizes in order to increase their chance of capturing prey. Different species have different methods of group hunting. A team of dolphins will try to make fish jump in the air where they are easy prey for the group. One group of lionesses would drive the fleeing prey to the second group that patiently awaits hidden. Recently, a few articles have paid attention to derive functional response to describe the cooperative hunting [2, 4, 8]. One of the first such articles is [8] by Cosner et. al. They considered several scenarios with prey and predator distribution during the hunt, with each scenario yielding one corresponding functional response. In one scenario, they assumed that prey forms herds or schools, while predator hunts in groups, forming a straight line. It is also assumed that, when one predator makes contact with a prey, it signals to all the other predators, which then converge around the prey herd, enclosing it. Prey in return disperses, allowing some, but not all of their population to escape. This sort of behavior is limited by the requirement that the line of foragers must be short enough to allow transmission of a signal, so the corresponding functional response gives a realistic description of hunting cooperation probably only at low to moderate predator group sizes. Thus, this assumptions yield in (1) the functional response

$$p(x, y) = \frac{Ce_0xy}{1 + hCe_0xy}. \tag{3}$$

Here, C is the amount of prey captured by predator per each attack, e_0 is attack rate coefficient of the predators, h is handling time per prey. Specific property of this functional response in compare with the conventional functional responses (see (i) to (ix)), is that the functional response has a monotonicity for both x and y, and moreover it increases when y increases. The monotonocity and the upper boundedness of this functional response can be characterized in the following way. As predator population grows large, their hunting becomes more efficient. But, overpopulation of predators will lead to decrease in their hunting efficiency, because if the line becomes too large for it to aggregate around the prey, the predation efficiently is not so good anymore.

There have been very few studies on mathematical models with the functional response (3). To our knowledge, Ryu et. al. in [21] were first to explore dynamics and bifurcation in the model (1) with the functional response (3). Considering the possibilities to ensure the coexistence of the two species, Shang et. al. in [23] included constant-yield harvesting of prey population in the mathematical model from [21]. Tiwari et. al. in [27] considered spatiotemporal model with included double Allee effect on prey population.

Shang et. al. [22] were first to consider the Leslie-Gower model with the functional response (3)

$$\begin{aligned}
\dot{x} &= rx\left(1 - \frac{x}{k}\right) - \frac{Cexy}{1 + hCexy}y \\
\dot{y} &= sy\left(1 - \frac{y}{nx}\right).
\end{aligned} \tag{4}$$

They showed that system is persistent, it can undergo both Hopf and generalized Hopf bifurcation around unique interior equilibria. Also, conditions for global asymptotic stability of the coexistence equilibrium have been determined.

Results in [21, 23, 27] imply that functional response (3), i.e. hunting cooperation included in this functional response, induces a strong Allee effect in predator population. A positive relationship between the per capita population growth rate and population size or density is called a demographic Allee effect (see [5]), first observed in 1930. by Allee [1]. In fact, the growth function in the logistic form is an positive function, while per capita growth rate decreases with density. However, for many species, low population density may induce many problems. For example, in species where mating or cooperation is necessary for successful reproduction and group defense, individuals may have difficulty finding mates or forming groups when the population size is too small. Additionally, in some cases, individuals may benefit from the presence of conspecifics, for example through increased vigilance against predators, and this benefit may decrease as the population size decreases. It turns out that the growth function of the low density population is not always positive, and it may be negative when the density of population is less than the minimum number necessary for the survival of the population, which is called the Allee threshold. Demographic Allee effects are characterized by a hump-shaped relationship between the per capita population growth rate and population size or density and can be classified into two types: strong Allee effect and weak Allee effect. A strong Allee effect indicates that populations may be particularly vulnerable to extinction at low densities. In fact, in the case of the strong Allee effect, there exists a threshold population level below which population growth rates become negative [9, 25]. Growth rate commence with negative values, but increase with density at low density until it reaches its maximum, and then it will decrease. In the case of the weak Allee effect, per capita growth rate remains positive at low population densities [9, 25]. A population with a weak Allee effect does not need any critical density for survival. Examples of species that exhibit a strong Allee effect include some social insects, such as ants and bees, where colony size is an important determinant of reproductive success, and some marine mammals, such as seals, where populations may be limited by the availability of suitable breeding sites. Examples of species that exhibit a weak Allee effect include some plants, where pollination or seed dispersal may be facilitated by a higher population density, and some fish, where the risk of predation may be reduced by schooling behavior.

With Allee effect included, the Leslie-Gower (2) becomes

$$
\begin{aligned}
\dot{x} &= rx\left(1 - \frac{x}{k}\right)(x - M) - p(x, y)y \\
\dot{y} &= sy\left(1 - \frac{y}{nx}\right)
\end{aligned}
\tag{5}
$$

The growth function $F(x) = rx(1 - x/k)(x - M)$ has an enhanced growth rate as the population increases above the Allee effect threshold M of the prey species. If $F(0) = 0$ and $F'(0) \geq 0$, as it is the case with $-k \leq M \leq 0$, then $F(x)$ represents prey population exhibits a weak Allee effect, whereas if $F(0) = 0$ and $F'(0) < 0$, as it is the case with $M > 0$, then $F(x)$ represents prey population exhibits a strong Allee effect. Arancibia-Ibarra et. al. in [3] considered system (5) with a strong Allee effect and Holling-type II functional response:

$$
\begin{aligned}
\dot{x} &= rx\left(1 - \frac{x}{k}\right)(x - M) - \frac{qxy}{x + a} \\
\dot{y} &= sy\left(1 - \frac{y}{nx}\right)
\end{aligned}
\tag{6}
$$

while Shang and Quao in [24] considered Leslie-Gower system (5) with a strong Allee effect and Holling-type IV functional response:

$$
\begin{aligned}
\dot{x} &= rx\left(1 - \frac{x}{K}\right)(x - M) - \frac{m_1 xy}{B + x^2} \\
\dot{y} &= sy\left(1 - \frac{y}{nx}\right)
\end{aligned}
\tag{7}
$$

The motive of this work is to investigate the dynamical behavior of the Leslie-Gower predator-prey model with Allee effect in growth of prey population and the function response (3). Our main goal is to see

how the both weak and strong Allee effect affect the dynamics of the prey-predator model (4) considered in [22]. Hence, the model to be studied in this paper is described as

$$
\begin{aligned}
\dot{x} &= rx\left(1 - \frac{x}{K}\right)(x - M) - \frac{Cexy}{1 + hCexy}y \\
\dot{y} &= sy\left(1 - \frac{y}{nx}\right),
\end{aligned}
\tag{8}
$$

Here, the positive constants r and K refer to the intrinsic growth rate of prey and the carrying capacity of the environment for the prey population, M is the Allee effect threshold, C is the amount of prey captured by predator per each attack, e_0 is attack rate coefficient of the predators, h is handling time per prey, s is intrinsic growth rate of predators and n measures the food quality of the prey for conversion into predator units. In order to reduce the number of parameters for stability and bifurcation analysis we scale the coordinates and constants with following transformations:

$$
\bar{t} = rKt, \quad \bar{x} = \frac{x}{K}, \quad \bar{y} = hCeKy, \quad m = \frac{M}{K}, \quad a = \frac{1}{Cerh^2K^3}, \quad b = \frac{s}{rK}, \quad c = \frac{s}{nrhCeK^3}.
$$

Dropping the bars, the system becomes:

$$
\begin{aligned}
\dot{x} &= x(1 - x)(x - m) - \frac{axy^2}{1 + xy} \\
\dot{y} &= y\left(b - c\frac{y}{x}\right).
\end{aligned}
\tag{9}
$$

It is important to note that $-1 \le m \le 1$, where $-1 \le m \le 0$ means that prey is under the influence of weak Allee effect, while for $0 < m \le 1$ it is under the influence of strong Allee effect.

The rest of this paper is organised as follows. In Section 2, we proved that system is biologically well-poised. Stability of the equilibria and dynamics of the system near origin were also studied. In Section 3, we analyse the existence and direction of bifurcations which include saddle-node bifurcation, Hopf bifurcation, generalized Hopf bifurcation and Bogdanov-Takens bifurcation of codimension 2. In Section 4 we provide numerical simulations and bifurcation diagrams for Bogdanov-Takens bifurcation as well as phase portraits for certain parameter values. Numerical simulations which include bifurcation diagrams and phase portraits were created using MATLAB software package MatCont (see [10]). Basins of attraction of multiple attractors were studied in Section 5. Phase portraits illustrated in this section were created using MATLAB program *pplane*8. Conclusion with proper biological interpretation is given in Section 6 and Appendixes are given in Section 7.

2. Basic properties and stability analysis

System (9) is not well defined for $x = 0$. For correct biological interpretation we only consider the model in the domain $\Omega = \{(x, y) : x > 0, y \ge 0\}$. The function, on the right hand side of the system (9) are continuously differentiable and locally Lipschitz in Ω, implying that the solutions of the initial value problem with non-negative initial conditions exist on the interval $[0, \tau), 0 < \tau \le +\infty$ and are unique.

2.1. Positivity and Dissipativeness

We can rewrite the system (9) as:

$$
\begin{aligned}
\dot{x} &= xf(x, y) = F(x, y) \\
\dot{y} &= yg(x, y) = G(x, y).
\end{aligned}
\tag{10}
$$

where

$$
f(x, y) = (1 - x)(x - m) - \frac{ay^2}{1 + xy}, \qquad g(x, y) = b - c\frac{y}{x}.
\tag{11}
$$

In this section, we prove that all the solutions of system (9), starting from a positive initial condition, remain positive and bounded.

2.1.1. Positivity

Theorem 2.1. *All solutions $(x(t), y(t))$ of the system (9) with positive initial values at $t = 0$, remain positive for all $t > 0$.*

Proof. Assume that $(x(0), y(0)) = (x_0, y_0)$ such that $x_0 > 0$ and $y_0 > 0$. From the right side equations of the system (10) we get:

$$x(t) = x_0 \exp\left(\int_0^t F(x(s), y(s))ds\right) > 0, \qquad y(t) = y_0 \exp\left(\int_0^t G(x(s), y(s))ds\right) > 0.$$

This proves the theorem. $\square$

2.1.2. Dissipativeness

Theorem 2.2. *System (9) is dissipative, and all solutions starting in Ω eventually enter region*
$$\Phi = \left\{(x, y) : 0 < x < 1, 0 \le y < \tfrac{b}{c}\right\}.$$

Proof. Let the $(x(t), y(t))$ be arbitrary positive solutions of the system (9) which satisfy positive initial condition $(x(0), y(0)) = (x_0, y_0)$, $x_0 > 0$, $y_0 > 0$. From the first equation in (10) we have

$$x(t) = x_0 \exp\left(\int_0^t F(x(s), y(s))ds\right), \quad t \ge 0. \tag{12}$$

Here, we observe two cases.

    I. Assume that $x_0 \le 1$ and prove that $x(t) \le 1$ for all $t \ge 0$. Suppose otherwise that there exists positive real numbers t_1, t_2 such that $x(t_1) = 1$ and $x(t) > 1$, $\forall t \in (t_1, t_2)$. Then, for all $t \in (t_1, t_2)$ we have that

$$\begin{aligned} x(t) &= x_0 \exp\left(\int_0^t F(x(s), y(s))ds\right) = x_0 \exp\left(\int_0^{t_1} F(x(s), y(s))ds\right) \exp\left(\int_{t_1}^t F(x(s), y(s))ds\right) \\ &= x(t_1) \exp\left(\int_{t_1}^t F(x(s), y(s))ds\right). \end{aligned} \tag{13}$$

    Since $1 - x(t) < 0$ and $x(t) - m > x(t) - 1 > 0$ for all $t \in (t_1, t_2)$, we conclude that $F(x(s), y(s)) < 0$, $\forall s \in (t_1, t_2)$. Hence, from (13), we have that $x(t) < x(t_1) = 1$, for all $t \in (t_1, t_2)$, which contradicts our hypothesis. Hence, $x(t) \le 1$ for all $t \ge 0$.

    II. Assume that $x_0 > 1$. Then, either

    (i) $x(t) > 1$ for all $t \ge 0$, implying that $F(x(s), y(s)) < 0$, $s \ge 0$ and so from (12) we get $x(t) < x(0) = x_0$, $t \ge 0$,

    or

    (ii) there exists some point $T > 0$, such that $x(T) = 1$, implying from the case (I) that $x(t) \le 1$, $\forall t > T$.

Hence, combining cases (I) and (II), we can say that any positive solution $x(t)$ which satisfy positive initial condition $x(0) = x_0 > 0$ satisfies $x(t) \le \max\{x(0), 1\}$ for all $t \ge 0$. If we denote $x_{sup} = \limsup_{t \to \infty} x(t)$, from the first equation of system (9), we get that

$$\dot{x} \le x(1 - x)(x - m) \le x(1 - x)(x_{sup} - m),$$

so that $\limsup_{t \to \infty} x(t) \le 1$. If we substitute $x = 1$ in the first equation of system (9), we get $\dot{x} = -\frac{ay^2}{1+y} < 0$. It follows from here that all trajectories enter and remain in the region $\Psi = \{(x, y) : 0 < x < 1, y \ge 0\}$. We further obtain from the second equation of system (9) that

$$\dot{y} = y\left(b - c\frac{y}{x}\right) \le y(b - cy) \Rightarrow \limsup_{t \to \infty} y(t) \le \frac{b}{c}.$$

Since all trajectories enter region Ψ, if we substitute $y = \frac{b}{c}$ in the second equation of system (9), we get $\dot{y} = y\left(b - \frac{b}{x}\right) < 0$. In other words, all trajectories that start in the region Ψ, eventually enter and remain in the region $\Phi = \left\{(x, y) : 0 < x < 1, 0 \leq y < \frac{b}{c}\right\}$. Therefore the model (9) is dissipative. $\square$

2.2. Equilibria and local stability

In this chapter we examine the axial equilibrium points (predator free equilibrium points) as well as possible number of interior equilibria (coexistence equilibrium points). We also examine the qualitative behaviour of the system near origin. Since the system (9) is not well defined for $x = 0$, in the case of the week Allee affect there is a unique axial equilibria $E_2(1, 0)$, while in the case of the strong Allee effect, there is two axial equilibria $E_1(m, 0)$ and $E_2(1, 0)$. The Jacobian matrix of the system (9) is given by

$$J(x, y) = \begin{pmatrix} 2x - 3x^2 + m(2x - 1) - \frac{ay^2}{(1+xy)^2} & a\left(-1 + \frac{1}{(1+xy)^2}\right) \\ c\frac{y^2}{x^2} & b - \frac{2cy}{x} \end{pmatrix}. \tag{14}$$

(i) The eigenvalues for the Jacobian matrix

$$J(m, 0) = \begin{pmatrix} m(1 - m) & 0 \\ 0 & b \end{pmatrix},$$

are $\lambda_1 = m(1 - m)$ and $\lambda_2 = b$. Since E_1 is biologically viable only when $m > 0$, we deduce that in that case, both eigenvalues are positive, meaning that E_1 is an unstable node.

(ii) The eigenvalues for the Jacobian matrix

$$J(1, 0) = \begin{pmatrix} -1 + m & 0 \\ 0 & b \end{pmatrix},$$

are $\lambda_1 = -1 + m$ and $\lambda_2 = b$. Since $b > 0$ and $-1 < m < 1$, we have that E_2 is always a hyperbolic saddle.

Interior equilibria lie in the intersection of non-trivial nullcines of the system (9). Nontrivial prey nullcline is given with $f(x, y) = 0$, while nontrivial predator nullcline is given by $g(x, y) = 0$, where functions f and g are given by (11). Predator nullcline can be rewritten as $y = bx/c$. If $E_p\left(x_p, y_p\right)$, is a positive equilibrium of system (9), then $y_p = bx_p/c$ and x_p is a positive root of the equation:

$$L(x) = x^4 + L_1 x^3 + L_2 x^2 + L_3 x + L_4, \tag{15}$$

where coefficients $L_i, i = \overline{1,4}$ are given with:

$$L_1 = -(1 + m), \quad L_2 = \frac{ab}{c} + \frac{c}{b} + m, \quad L_3 = -\frac{c(1 + m)}{b}, \quad L_4 = \frac{cm}{b}.$$

Possible number of interior equilibrium points of system (9) and parametric restrictions under which equilibrium points exist are very difficult to find. Therefore we must observe possible intersections of non-trivial predator and prey nullclines. Non-trivial predator nullcline is linear strongly increasing function and it intersects x-axis in two points: E_1 and E_2. Numerical simulations show that this nullcline in the first quadrant has parabolic shape with one maximum at x_{max}. To determine the number of positive and unique equilibria, we observe cases of weak and strong Allee effect separately. To discuss the local asymptotic stability properties of the interior equilibrium points $E_p(x_p, y_p)$, where $y_p = bx_p/c$, we observe the Jacobian matrix of the system (9) at arbitrary interior point E_p. Since $f(x_p, y_p) = g(x_p, y_p) = 0$ the Jacobian matrix is given by

$$J_p = J(x_p, y_p) = \begin{pmatrix} x_p \frac{\partial f}{\partial x}(x_p, y_p) & x_p \frac{\partial f}{\partial y}(x_p, y_p) \\ y_p \frac{\partial g}{\partial x}(x, y_p) & y_p \frac{\partial g}{\partial y}(x_p, y_p) \end{pmatrix} = \begin{pmatrix} J_{11}(E_p) & J_{12}(E_p) \\ J_{21}(E_p) & J_{22}(E_p) \end{pmatrix},$$

implying that

$$J_p = J(x_p, y_p) = \begin{pmatrix} (1 + m - 2x_p)x_p + \frac{ab^3 x_p^4}{c(c+bx_p^2)^2} & a\left(\frac{c^2}{(c+bx_p^2)^2} - 1\right), \\ \frac{b^2}{c} & -b \end{pmatrix}$$

so that the trace and the determinant of the Jacobian matrix J_p are given by:

$$trace(J_p) = (1 + m - 2x_p)x_p + \frac{ab^3 x_p^4}{c(c+bx_p^2)^2} - b, \quad det(J_p) = bx_p^2\left(2 + \frac{2ab^2}{\left(c+bx_p^2\right)^2}\right) - bx_p(m+1). \tag{16}$$

Therefore, for every internal equilibrium, for elements of the Jacobian matrix J_p we have that $J_{21}(E_p) > 0$, $J_{22}(E_p) < 0$. It remain to determine the sign of $J_{11}(E_p)$ and $J_{12}(E_p)$.

2.2.1. Weak Allee Effect

In this case, non-trivial predator nullcline always intersects the prey nullcline. Since non-trivial predator nullcline is strongly increasing, there exists only one intersection in the first quadrant. This intersection corresponds to unique interior equilibrium point $E_3(x_3, y_3)$, shown on Figure 1. Let's emphasize that since $m < 0$, point $E_2(m, 0)$, at which non-trivial predator nullcline intersects x-axis, falls outside of the first quadrant. Therefore, non-trivial predator nullcline will have intersection with positive part of y-axis.
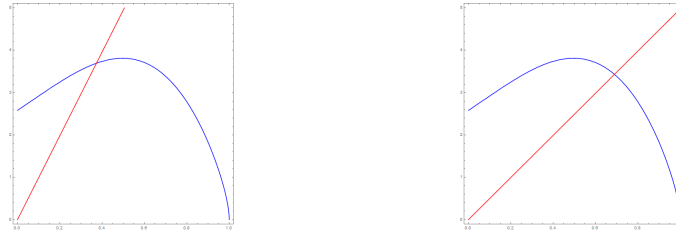
Figure 1: *Relative positions of prey nullcline (blue colored) and predator nullcline (red colored) in the case of weak Allee effect. Their intersection corresponds to the unique interior equilibrium point $E_3(x_3, y_3)$.* **(a)** *Case when $x_3 < x_{max}$.* **(b)** *Case when $x_3 > x_{max}$.*

Since the gradient of the tangent of curves $f(x, y) = 0$ and $g(x, y) = 0$ at some point (x_0, y_0) are respectively

$$\frac{dy^{(f)}}{dx}(x_0) = -\frac{\frac{\partial f}{\partial x}(x_0, y_0)}{\frac{\partial f}{\partial y}(x_0, y_0)}, \quad \frac{dy^{(g)}}{dx}(x_0) = -\frac{\frac{\partial g}{\partial x}(x_0, y_0)}{\frac{\partial g}{\partial y}(x_0, y_0)}, \tag{17}$$

we can express the determinant of J_3 as follows:

$$\begin{aligned} det(J_3) &= x_3 y_3 \left(\frac{\partial f}{\partial x}(x_3, y_3)\frac{\partial g}{\partial y}(x_3, y_3) - \frac{\partial f}{\partial y}(x_3, y_3)\frac{\partial g}{\partial x}(x_3, y_3)\right) \\ &= x_3 y_3 \frac{\partial f}{\partial y}(x_3, y_3)\frac{\partial g}{\partial y}(x_3, y_3)\left(\frac{dy^{(g)}}{dx}(x_3) - \frac{dy^{(f)}}{dx}(x_3)\right) \end{aligned} \tag{18}$$

The stability of the equilibrium point will be determined by observing the sign of the elements of the Jacobian matrix J_3 and the expressions of $trace(J_3)$ and $det(J_3)$ given by (16) and (18). Here we distinguish two subcases.

- Observe the case when $x_3 < x_{max}$ (see Figure 1-(a)). Below the non-trivial prey nullcline we have that $f(x, y) > 0$ and above it we have $f(x, y) < 0$. It follows from here that $f(x_3 - \triangle x, y_3) < 0$ and

$f(x_3 + \triangle x, y_3) > 0$. This implies that $\frac{\partial f}{\partial x}(x_3, y_3) > 0$. With similar procedure, one can find sign of $\frac{\partial f}{\partial y}(x_3, y_3) > 0$, so that using that $x_3 > 0$ and $y_3 > 0$, signs of elements in the matrix J_3 are as follows:

$$Sign(J_3) = \begin{pmatrix} + & - \\ + & - \end{pmatrix}. \tag{19}$$

At E_3, slope of the predator non-trivial nullcline is greater than the slope of prey non-trivial nullcline. Therefore, we have that $\frac{dy^{(g)}}{dx}(x_3) - \frac{dy^{(f)}}{dx}(x_3) > 0$. Considering the signs of other factors in (18), we deduce that $det(J_3) > 0$. Hence the stability of this E_3 depends upon the sign of $trace(J_3)$. If $trace(J_3) < 0$, then E_3 is locally asymptotically stable, otherwise it is unstable.

- Observe the case when $x_3 > x_{max}$ (see Figure 1-(b)). Using similar approach as in the previous case, we determine that signs of the elements of the Jacobian matrix J_3 are given by:

$$Sign(J_3) = \begin{pmatrix} - & - \\ + & - \end{pmatrix}. \tag{20}$$

Similarly, we have that $det(J_3) > 0$. In this case, however, it is clear that $tr(J_3) < 0$. Therefore, equilibrium point E_3 is always locally asymptotically stable.

2.2.2. Strong Allee Effect

In the case of strong Allee effect, there are three possible outcomes when it comes to predator and prey non-trivial nullcline intersections, as shown in Figure 2. The number of intersections varies from zero to two. If nontrivial nullclines do not intersect (Figure 2-(a)), the system has no interior equilibria. Prey and predator non-trivial nullcline touch each other at the unique interior equilibrium (Figure 2-(b)). There exist two interior equilibria $E_4(x_4, y_4)$ and $E_5(x_5, y_5)$, where $x_4 < x_5$, if non-trivial nullclines intersect in the first quadrant.

Figure 2: *Number of equilibrium points in the case of strong Allee effect, based on relative positions of prey and predator non-trivial nullclines. Number of equilibrium points varies from zero to two. If non-trivial nullclines intersect in the first quadrant, we observe two cases:* **(c)** $x_4 < x_5 < x_{max}$; **(d)** $x_4 < x_{max} < x_5$.

Discussing the stability of E_4 (see Figure 2-(c) and Figure 2-(d)) we follow similar procedure as in the case of weak Allee effect and find that signs of the elements of the Jacobian matrix J_4 at equilibrium point E_4 are as follows:

$$Sign(J_4) = \begin{pmatrix} + & - \\ + & - \end{pmatrix}.$$

Prey non-trivial nullcline has greater slope than the predator non-trivial nullcline at equilibrium point E_4. Therefore, $\frac{dy^{(g)}}{dx}(x_4) - \frac{dy^{(f)}}{dx}(x_4) < 0$. Considering the signs of other entries in J_4, we deduce that $det(J_4) < 0$. This means that E_4 is always a hyperbolic saddle. For the stability of E_5, as in the case of weak Allee effect we observe two separate subcases: $x_4 < x_5 < x_{max}$ (see Figure 2-(c)) and $x_4 < x_{max} < x_5$ (see Figure 2-(d)), and signs of the elements of the Jacobian matrix J_5 are the same as $Sign(J_3)$ in (19) and (20), respectively, implying the same conclusion about the stability of this equilibrium point in these two cases.

2.2.3. Qualitative behaviour near the origin of the system

In order to determine in which cases the extinction of both populations can be avoided, we explore qualitative dynamics of the system (9) in the neighbourhood of the origin and in the cases where the origin acts as an local attractor, we study its basin of attraction. The basin of attraction $\mathcal{B}(x^\star)$ of the stable equilibra $x^\star$ is the set of all points in phase space that converge to $x^\star$ in forward time.

We introduce time scaling $d\tau = \frac{dt}{x(1+xy)}$ to transform system (9) into

$$
\begin{aligned}
\dot{x} &= x^2\big((1-x)(x-m)(1+xy) - ay^2\big) \\
\dot{y} &= y\big(bx(1+xy) - cy(1+xy)\big),
\end{aligned}
\tag{21}
$$

which is topologically equivalent to the system (9). If we set $x = 0$, from the second equation of the system (21), we get $\dot{y} = -cy^2 < 0$. Therefore, y-axis is an invariant line which converges to the origin. On the other hand, if we set $y = 0$, we get $\dot{x} = x^2(1-x)(x-m)$. In the case when $m < 0$, orbits with initial values on the x-axis will diverge from the origin provided that $x(0) < 1$. In the case when $m > 0$, orbits along the x-axis will converge towards the origin only if $x(0) < m$, otherwise they will diverge. The case when $m = 0$ is analysed later. The Jacobian matrix of system (21), calculated at the origin is zero matrix, meaning that the origin is non-hyperbolic. To desingularize the origin, we use the blow-up method described in [11]. More precisely, we blow-up the origin in x-direction. Blow-up in y-direction is omitted due to not providing new insights into dynamics of the system near origin. Using the transformations

$$
x = u, \qquad y = uv, \qquad \tau = t/x
\tag{22}
$$

the origin is blown up into the entire u-axis. System (21) is transformed into

$$
\begin{aligned}
\frac{du}{d\tau} &= u\big(u + m(u-1)(u^2v+1) - u^2(1 + (u-1)uv + av^2)\big) \\
\frac{dv}{d\tau} &= v\big(b + m - (m+1)u - cv + u^2 + u^2v(b + m - (1+m)u + u^2 + v(a-c))\big).
\end{aligned}
\tag{23}
$$

System (23) has two equilibria on v-axis: $U_0(0,0)$ and $U_1\left(0, \frac{b+m}{c}\right)$. Jacobian matrices of the system (23) in U_0 and U_1 are given with

$$
J_0 = J(0,0) = \begin{pmatrix} -m & 0 \\ 0 & b+m \end{pmatrix}, \quad J_1 = J\left(0, \frac{b+m}{c}\right) = \begin{pmatrix} -m & 0 \\ -\frac{(m+1)(b+m)}{c} & -b-m \end{pmatrix}.
$$

The Jacobian matrix J_0 has two real eigenvalues $\lambda_1 = -m$ and $\lambda_2 = b + m$, while the eigenvalues of the Jacobian matrix J_1 are $\lambda_3 = -m$ and $\lambda_4 = -(b+m)$. We observe the following cases:

$$
(1)\ b + m > 0 \qquad (2)\ b + m < 0 \qquad (3)\ b + m = 0 \qquad (4)\ m = 0.
$$

(Case 1.) $b + m > 0$. We separate two subcases.

(1-a) In the case when $m > 0$, we have that $\lambda_1 < 0$ and $\lambda_2 > 0$, indicating that U_0 is a saddle. Right branch of the stable manifold of U_0 is contained in the u-axis, while the upper branch of the unstable manifold is contained in the v-axis. Since $\lambda_3 < 0$ and $\lambda_4 < 0$, U_1 is locally asymptotically stable node. Two branches of the stable manifold of U_1 tangent to the fast stable subspace of the linear system $w' = J_1 w$ are contained in the v-axis, while the one branch of the stable manifold of U_1 tangent to the slow stable subspace of the linear system at U_1, belongs to the open first quadrant. Dynamics of the system (23) are depicted in the Figure 3-(a) (note that the curve $W^s(U_1)$ is a local approximation of the stable manifold of U_1). By taking the inverse transformations

$$
u = x, \qquad v = \frac{y}{x}, \qquad t = \tau u
\tag{24}
$$

the line $u = 0$ is collapsed to the origin of the system, while the line $v = 0$ is mapped to $y = 0$ and the curve $W^s(U_1)$ is mapped to some curve $\Gamma^s(E_1)$ in the open first quadrant.

Thus, the basin of attraction $\mathcal{B}(U_1)$ is mapped to the open region Ω. Since time rescaling preserves time-orientation of the orbits in the first quadrant, every orbit in this open region approaches to the origin of the system (9) in the forward time. Hence, we deduce that the origin of the system (9) is a *local attractor* with a parabolic attracting sector in the first quadrant. Dynamics of the system (9) in this case is depicted in the Figure 3-(b).
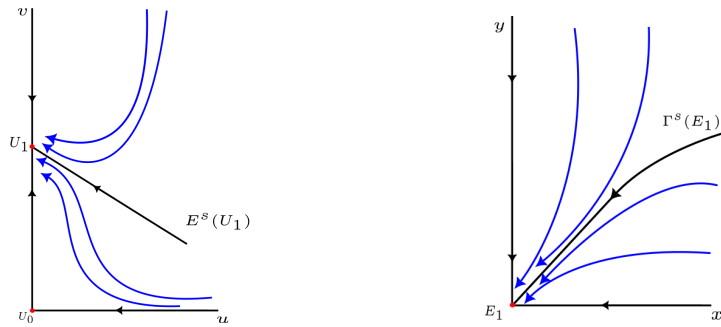
Figure 3: *Dynamics of the system near the origin when $b + m > 0$ and $m > 0$.* **(a)** *For the system* (23). **(b)** *For the system* (9).

(1-b) In the case when $m < 0$, we have that $\lambda_1 > 0$ and $\lambda_2 > 0$, which indicates that U_0 is an unstable node. One branch of the unstable manifold of U_0, tangent to the fast stable subspace of the linear system at U_0 is contained in the u-axis, while the one branch of the unstable manifold of U_0, tangent to the slow stable subspace of the linear system at U_0 is contained in the v-axis. At the same time, $\lambda_3 > 0$ and $\lambda_4 < 0$, indicating that U_1 is a saddle. Both branches of the stable manifold of U_1 are contained in the v-axis, while the one branch of the unstable manifold of U_1 belongs to the open first quadrant. Dynamics of the system (23) is depicted in the Figure 4-(a).

By taking the inverse transformations (24), the curve $W^u(U_1)$ which is a local approximation of the unstable manifold of U_1 is mapped to some curve $\Gamma^u(E_1)$, which belongs to the region Ω. Orientation of the orbits in the first quadrant is preserved, and therefore we deduce that the origin of the system (9) is a *local repeller* with one hyperbolic sector and one parabolic repelling sector in the first quadrant. Curve $\Gamma^u(E_1)$ and y−axis serve as separatrix curves for a hyperbolic sector. Dynamics of the system (9) in this case is depicted in the Figure 4-(b).
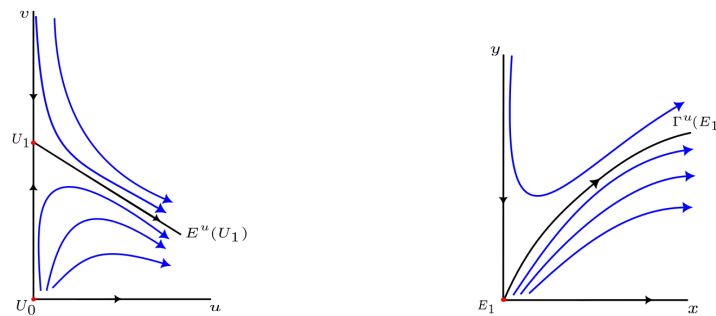
Figure 4: *Dynamics of the system near the origin when $b + m > 0$ and $m < 0$:* **(a)** *for the system* (23) **(b)** *for the system* (9).

(Case 2.) $b + m < 0$. Since we know that $b > 0$, the case where $b + m < 0$ is only possible when $m < 0$. In

this case, equilibrium point U_0 is a saddle, while equilibrium point U_1 is an unstable node. However, the second coordinate of U_1 is less than zero and both branches of the unstable manifold of U_1 are contained in the exterior of the first quadrant. Hence, by 'blowing-down' to the system (9), we conclude that dynamic of the systems (23) and (9) is similar, depicted in the Figure 5-(a) and 5-(b), respectively. The origin is a *repeller* with a hyperbolic sector in Ω whose separatrices are axis.
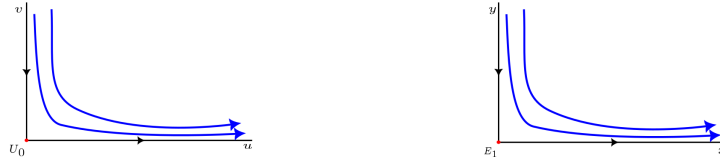
Figure 5: *Dynamics of the system near the origin when $b + m < 0$: **(a)** For the system* (23). ***(b)** For the system* (9).

Next, we determine the dynamics of system (23) when two special cases can occur: $b + m = 0$ and $m = 0$.

(Case 3.) If $b + m = 0$, equilibrium points U_1 collides with the origin U_0. Eigenvalues of the J_0 are $\lambda_1 = b > 0$ and $\lambda_2 = 0$, meaning that U_0 is non-hyperbolic. In this case, one branch of the unstable manifold $W^u(U_0)$ is contained in the u-axis, while the center manifold $W^c(U_0)$ can be locally approximated with v-axis. From centre manifolds theory, the dynamics near equilibrium U_0 is dominated by the vector field restricted to its centre manifold $\dot{v} = -cv^2$. It follows that the origin of the system (23) is a *saddle-node* with a hyperbolic sector in the first quadrant. Dynamics of the systems (23) and (9) therefore match with the ones shown in the Figure 5.

(Case 4.) If $m = 0$, there exist two equilibrium points, $U_0(0,0)$ and $U_1\left(0, \frac{b}{c}\right)$. Eigenvalues of J_0 are $\lambda_1 = b > 0$ and $\lambda_2 = 0$, while eigenvalues of J_1 are $\lambda_3 = 0$ and $\lambda_4 = -b < 0$. Both U_0 and U_1 are non-hyperbolic.

One branch of the unstable manifold $W^u(U_0)$ is contained in the v-axis, while the central manifold $W^c(U_0)$ near U_0 can locally be approximated as u-axis. The dynamics of the system (23) near equilibrium U_0 dominated by the vector field restricted to its centre manifold

$$\dot{u}\Big|_{W^c(U_0)} = u^2 - u^3.$$

It follows that U_0 is a saddle-node of the system (23), with a hyperbolic sector in the first quadrant.

One branch of the stable manifold $W^s(U_1)$ is contained in the v-axis, while the central manifold $W^c(U_1)$ near U_1 can locally be approximated with:

$$\widehat{G} = \left\{(u, v) : v = h(u) = \frac{b}{c} + \frac{ab^3 + c^2(1 + b)}{bc}u^2 + \frac{5ab^3 + c^2(1 + 3b)}{b^2}u^3 + O(u^4)\right\}$$

The dynamics of the system (23) near equilibrium U_1 restricted to the central manifold is given by:

$$\dot{u}\Big|_{W^c(U_1)} = cu^2 - \left(1 + \frac{ab^2}{c^2}\right)u^3 + O(u^4).$$

Therefore, equilibrium point U_1 is saddle-node with two hyperbolic sectors in the first quadrant, while the curve $\widehat{G}$ serves as a local separatrix between two sectors. The desired dynamics of the system (9) is obtained by 'blowing-down' the dynamics of the system (23) back to the system (9). In fact, by "blowing-down" $W^c(U_0)$, one obtains the x−axis, while in a neighbourhood of the origin in (9), using by (24), the inverse image of the curve $\widehat{G}$ is the invariant curve

$$\Gamma = \left\{(x, y) : y = \frac{b}{c}x + \frac{ab^3 + c^2(1 + b)}{bc}x^3 + \frac{5ab^3 + c^2(1 + 3b)}{b^2}x^4 + O(x^5)\right\}$$

Therefore, we get that the origin of the system (9) is a *local repeller* with one hyperbolic sector and one parabolic repelling sector in the first quadrant. Curve Γ and y-axis serve as separatrices for a hyperbolic sector. Dynamics of the system (9) matches the one depicted in the Figure 4-(b).

In conclusion, in the case of strong Allee effect, with $m > 0$, the origin is always a local attractor; see the basin of attraction $\mathcal{B}(0,0)$ in Figure 3-(b). Earlier it was stated that number of interior equilibria in system (9), when under the influence of strong Allee effect, varies between zero and two. If the system has no interior equilibria, given that axial equilibria E_1, E_2 are unstable and all solution of the system with positive initial value end up in the bounded region Φ, by Poincarè-Bendixon theorem, the origin is globally asymptotically stable in the first quadrant.

On the other hand, for a weak Allee effect, with $m \leq 0$, extinction is avoided, shown in Figures 4-(b) and 5-(b). Given that predator-free equilibria E_3 is hyperbolic saddle, system will be persistent.

3. Bifurcation analysis

3.1. Saddle-node bifurcation

Analyzing the relative position of non-trivial nullclines in the case of strong Allee effect, we concluded that number of interior equilibria varies from zero to two. It is clear that, under some conditions, saddle-node bifurcation occurs. We consider the existence of saddle-node bifurcation around interior equilibrium by taking m as bifurcation parameter. The bifurcation threshold value for which saddle-node bifurcation occurs is denoted by m_{sn}. Interior equilibria E_4 and E_5 will collide to $E_{sn}(x_{sn}, y_{sn})$ when $L(x)$, given by (15), has double root in the interval $(m, 1)$. We assume that the polynomial $L(x)$ has a positive double root $x_{sn} \in (m, 1)$ for some threshold value $m = m_{sn}$. Then, $L(x_{sn}) = L'(x_{sn}) = 0$ and $L''(x_{sn}) \neq 0$. Geometrically, this means that the prey non-trivial nullcline touches the predator non-trivial nullcline at the point $E_{sn}(x_{sn}, y_{sn})$. Since the slopes of non-trivial nullclines are same at E_{sn}, we have that

$$\left.\frac{dy^{(f)}}{dx}(x_{sn})\right|_{m=m_{sn}} = \left.\frac{dy^{(g)}}{dx}(x_{sn})\right|_{m=m_{sn}},$$

which using (18) implies that $\det(J(x_{sn}, y_{sn}))\big|_{m=m_{sn}} = 0$. Therefore, $J_{SN} = J(x_{sn}, y_{sn})\big|_{m=m_{sn}}$ has zero eigenvalue.

Since saddle-node bifurcation is only possible in the case of the strong Allee effect, we need to show that threshold value of parameter m falls in the interval $(0, 1)$. To verify this, we simply need to check that, for $m = m_{sn}$, slope of prey non-trivial nullcline is positive at the point E_{sn}. From (17) we get that:

$$\left.\frac{dy^{(f)}}{dx}(x_{sn})\right|_{m=m_{sn}} = -\left.\frac{\frac{\partial f}{\partial x}(x, y)}{\frac{\partial f}{\partial y}(x, y)}\right|_{m=m_{sn}, x=x_{sn}, y=y_{sn}} = \frac{b}{c} > 0,$$

which confirms that $m_{sn} \in (0, 1)$.

To check corresponding transversality conditions of saddle-node bifurcation, we determine the eigenvectors corresponding to the zero eigenvalue of matrices J_{SN} and J_{SN}^T:

$$v = \begin{pmatrix} v_1 \\ v_2 \end{pmatrix} = \begin{pmatrix} \frac{c}{b} \\ 1 \end{pmatrix}, \quad w = \begin{pmatrix} w_1 \\ w_2 \end{pmatrix} = \begin{pmatrix} -\frac{(c+bx_{sn}^2)^2}{ax_{sn}^2(2c+bx_{sn})} \\ 1 \end{pmatrix}.$$

The vector field of the system (10) is given by $\mathcal{F}(x, y) = (xf(x, y), yg(x, y))^T$. Differentiating the vector function $\mathcal{F}(x, y)$ with respect to the bifurcation parameter m we obtain the function $\mathcal{F}_m(x, y) = (x\frac{\partial f(x,y)}{\partial m}, 0)^T$. The transversality conditions for saddle-node bifurcation are verified as follows:

$$w^T\mathcal{F}_m(x, y)\big|_{m=m_{sn}, x=x_{sn}, y=y_{sn}} = -\frac{(x_{sn}-1)(c+bx_{sn}^2)^2}{ax_{sn}(2c+bx_{sn}^2)} \neq 0,$$

$$w^T D^2\mathcal{F}(x, y)(v, v)\big|_{m=m_{sn}, x=x_{sn}, y=y_{sn}} = \frac{2c^2(ab^2(c-3bx_{sn}^2) + (c+bx_{sn}^2)^3)}{ab^2 x_{sn}(c+bx_{sn}^2)(2c+bx_{sn}^2)}.$$

Therefore, by Sotomayor theorem [19], the system (9) undergoes saddle-node bifurcation if $ab^2(3bx_{sn}^2 - c) \neq (c + bx_{sn}^2)^3$ and the following theorem is proved.

Theorem 3.1. *System* (9) *undergoes saddle-node bifurcation with respect to the bifurcation parameter m, through which two interior equilibria E_4 and E_5 collide to $E_{sn}(x_{sn}, y_{sn})$ at bifurcation threshold $m = m_{sn}$, if $ab^2(3bx_{sn}^2 - c) \neq (c + bx_{sn}^2)^3$*

3.2. Hopf bifurcation

When discussing the stability of the interior equilibria E_3 for weak Allee effect, we concluded that E_3 is always locally asymptotically stable if $x_3 > x_{max}$. The change of stability of the interior equilibrium point E_3 may occur if $x_3 < x_{max}$, in which case stability depends on the sign of the trace of the Jacobian matrix J_3. In the same way, in the case of strong Allee effect, the change of stability of the interior equilibrium point E_5 may occur if $x_5 < x_{max}$. This suggests that Hopf bifurcation occurs at one interior equilibrium point, regardless of the intensity of Allee effect. We explore the possibility of occurrence of Hopf bifurcation and its direction around the interior equilibrium point $E_h(\widehat{x}(m), \widehat{y}(m))$, where $\widehat{y}(m) = b\widehat{x}(m)/c$, with respect to the bifurcating parameter m. We investigate the threshold value m_h and the corresponding transversality conditions. The Jacobian matrix at $(\widehat{x}(m), \widehat{y}(m))$ is given by

$$J_H = J\left(\widehat{x}(m), \widehat{y}(m)\right) = \begin{pmatrix} \widehat{x}(m)\left(1 + m - 2\widehat{x}(m) + \frac{ab^3\widehat{x}(m)^3}{c(c+b\widehat{x}(m)^2)^2}\right) & a\left(\frac{c^2}{(c+b\widehat{x}(m)^2)^2} - 1\right) \\ b^2/c & -b \end{pmatrix}.$$

Theorem 3.2. *The interior equilibrium point $E_h(\widehat{x}(m), \widehat{y}(m))$ changes its stability through the Hopf-bifurcation at the threshold $m = m_h$ such that*

$$\text{(i)} \;\; T(m)\Big|_{m=m_h} = 0 \qquad \text{(ii)} \;\; D(m)\Big|_{m=m_h} > 0 \qquad \text{(iii)} \;\; \frac{dT(m)}{dm}\Big|_{m=m_h} \neq 0, \tag{25}$$

where $T(m) = trace(J_H)$ and $D(m_h) = det(J_H)$.

Proof. The Hopf bifurcation threshold value m_h is obtained from $T(m) = 0$, so that $m = m_h$ is a solution of the equation:

$$(1 + m - 2\widehat{x}(m))\widehat{x}(m) + \frac{ab^3\widehat{x}(m)^4}{c(c + b\widehat{x}(m)^2)^2} - b = 0.$$

It follows from the discussion in Sections 2.2.1 and 2.2.2 that $D(m_h) > 0$, therefore condition (ii) is satisfied. If (i) and (ii) hold, the characteristic equation $\lambda^2 + D(m_h) = 0$ has two purely imaginary roots $\lambda_{1,2} = \pm\theta_0 = \pm i\sqrt{D(m_h)}$. To check the transversality condition for Hopf bifurcation let at any point m in the neighbourhood of m_h the eigenvalues of the Jacobian matrix are $\lambda_{1,2} = \xi(m) \pm \theta(m)$, where $\xi(m) = \frac{1}{2}T(m)$ and $\theta(m) = \frac{1}{2}\sqrt{4D(m) - T^2(m)}$. Then, if

$$\frac{d}{dm}\xi(m)\Big|_{m=m_h} = \frac{1}{2}\frac{dT(m)}{dm}\Big|_{m=m_h} \neq 0$$

the transversality condition is satisfied and the system undergoes Hopf-bifurcation at $m = m_h$ satisfying (25). $\square$

The stability of the limit cycle is determined by the sign of the first Lyapunov coefficient. We determine the expression for the first Lyapunov coefficient ℓ_1, by using the method described in Kuznetsov [14]. Hopf-bifurcation is supercritical if $\ell_1 < 0$ and it is subcritical if $\ell_1 > 0$. It is to be noted that when $\ell_1 = 0$, the system exhibits generalized Hopf-bifurcation (Bautin bifurcation). Since it is difficult to provide the explicit parametric expression for the coordinates of the interior equilibrium point, an analytic expression for the threshold as well as condition for parameters under which sign of the first Lyapunov coefficient can change, are very difficult to obtain. However, numerically, we have investigated that in both cases of strong (see Figures 6,7) and weak Allee effect (see Figures 8,9), the system undergoes both supercritical and subcritical Hopf-bifurcation as we vary the bifurcation parameter m.

- Fix parameter values $a = 0.669286$, $b = c = 0.15$. Threshold value is $m_h = 0.23569$ at which system (9) has an equilibrium point $E_h(0.490672, 0.490672)$ with eigenvalues $\lambda_{1,2} = \pm 0.112609i$. First Lyapunov coefficient at equilibrium point E_h for these parameter values is equal to $\ell_1 = 0.291261 > 0$. Therefore, subcritical Hopf bifurcation occurs around E_h. For fixed value $m = 0.2361 > m_h$, system (9) has two interior equilibrium points $E_3(0.34421, 0.34421)$ and $E_4(0.489448, 0.489448)$. Eigenvalues of the Jacobian matrix calculated at E_3 are $\lambda_1 = 0.121963$ and $\lambda_2 = -0.0759361$, meaning E_3 is a saddle point. Eigenvalues corresponding to the equilibrium point E_4 are $\lambda_{1,2} = 0.000442971 \pm 0.111451i$, meaning E_4 is unstable focus. Phase portrait is shown on Figure 6-(a). As $m = 0.2353$ decreases below it's threshold value m_h, $E_4(0.491814, 0.491814)$ becomes locally asymptotically stable focus, while unstable limit cycle appears around it, as shown on Figure 6-(b).
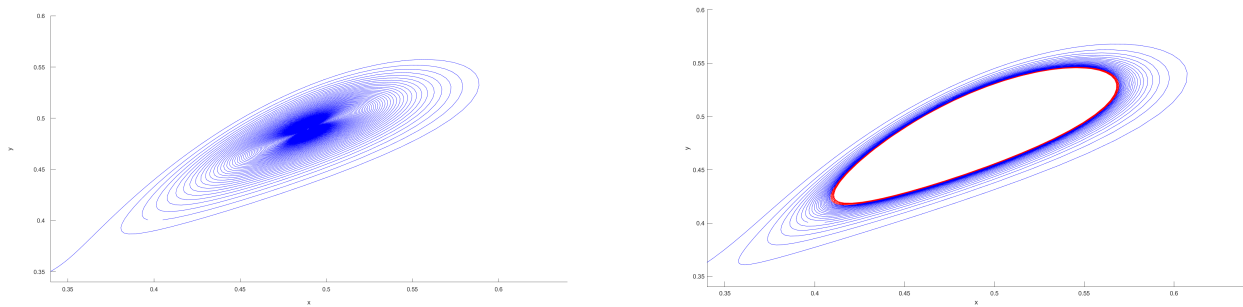
Figure 6: SUBCRITICAL HOPF BIFURCATION IN THE CASE OF STRONG ALLEE EFFECT: *Phase portraits of the system (9) for fixed values of parameters $a = 0.669286$, $b = c = 0.15$. The system exhibits subcritical Hopf-bifurcations at $m_h = 0.23569$. (a) Fixed value $m = 0.2361 > m_h$. Equilibrium point is unstable focus and there is no limit cycles. (b) Fixed value $m = 0.2353 < m_h$. Unstable limit cycle around stable interior equilibrium point.*

- Fix parameter values $a = 0.901249$, $b = c = 0.15$. Threshold value is $m_h = 0.174919$ at which system (9) has an equilibrium point $E_h(0.448322, 0.448322)$ with eigenvalues $\lambda_{1,2} = \pm 0.137704i$. First Lyapunov coefficient at equilibrium point E_h is equal $\ell_1 = -0.699092 < 0$. Therefore, supercritical Hopf bifurcation occurs around E_h. For fixed value $m = 0.1756 > m_h$, system (9) has two interior equilibrium points $E_3(0.240457, 0.240457)$ and $E_4(0.446984, 0.446984)$. Equilibrium point E_3 is saddle with eigenvalues $\lambda_1 = 0.115617$ and $\lambda_2 = -0.0958825$. Equilibrium point E_4 is unstable focus with eigenvalues $\lambda_{1,2} = 0.000438404 \pm 0.136541i$. For $m = 0.1756 > m_h$ above its threshold value, E_4 is unstable focus around which exists stable limit cycle, depicted on Figure 7-(a). As m decreases below it's threshold value m_h, for $m = 0.1745 < m_h$, limit cycle disappears while $E_4(0.449143, 0.449143)$ becomes locally asymptotically stable focus, as shown on Figure 7-(b).
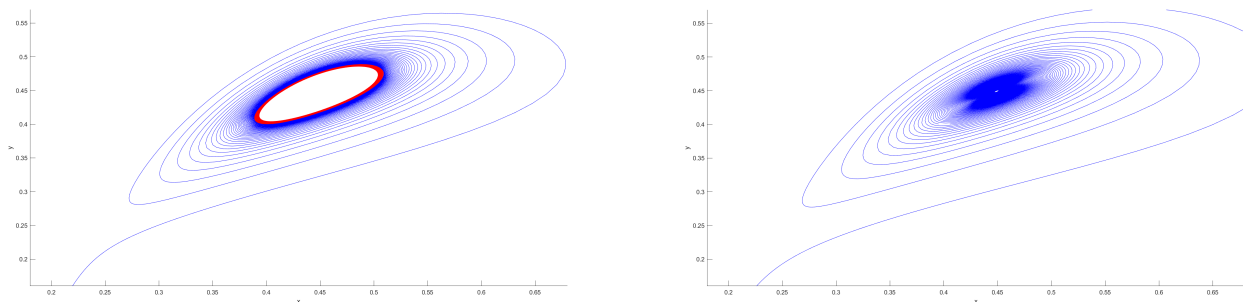
Figure 7: SUPERCRITICAL HOPF BIFURCATION IN THE CASE OF STRONG ALLEE EFFECT: *Phase portraits of the system (9) for fixed values of parameters $a = 0.901249$, $b = c = 0.15$. The system exhibits supercritical Hopf-bifurcations at $m_h = 0.174919$. a) Fixed value $m = 0.1756 > m_h$. Stable limit cycle around unstable interior equilibrium point. b) Fixed value $m = 0.1745 < m_h$. Equilibrium point is locally asymptotically stable focus and there is no limit cycles.*

- Fix parameter values $a = 14$, $b = c = 0.08$. Threshold value is $m_h = -0.086351$ at which system (9) has an equilibrium point $E_h(0.11313, 0.11313)$ with eigenvalues $\lambda_{1,2} = \pm0.147402i$. First Lyapunov coefficient at equilibrium point E_h for these parameter values is equal to $\ell_1 = 1.17687 > 0$. Therefore, subcritical Hopf bifurcation occurs around E_h. For fixed value $m = -0.11 < m_h$, system (9) has one interior equilibrium point $E_3(0.12139, 0.12139)$. Eigenvalues corresponding to the equilibrium point E_3 are $\lambda_{1,2} = 0.000759134 \pm 0.16053i$, meaning E_3 is unstable focus, depicted on Figure 8-(a). As m increases above it's threshold value m_h, for $m = -0.07 > m_h$, $E_3(0.106814, 0.106814)$ becomes locally asymptotically stable focus, while unstable limit cycle appears around it, as shown on Figure 8-(b).
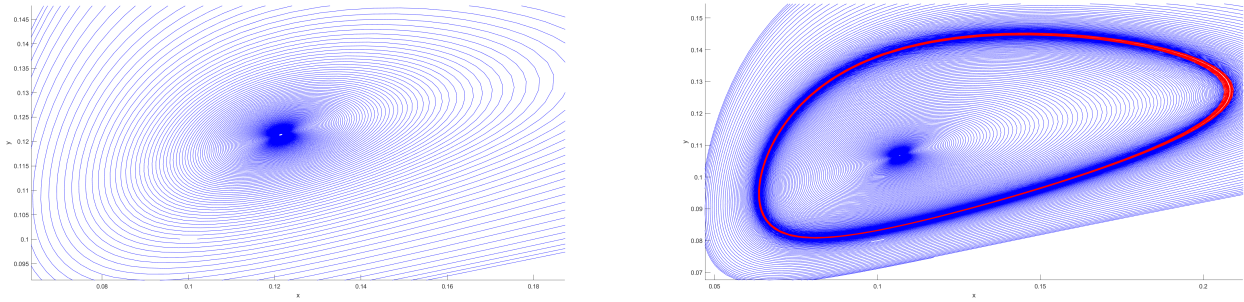
Figure 8: SUBCRITICAL HOPF BIFURCATION IN THE CASE OF WEAK ALLEE EFFECT: *Phase portraits of the system* (9) *for fixed values of parameters $a = 14$, $b = c = 0.08$. The system exhibits subcritical Hopf-bifurcations at $m_h = -0.086351$. (a) Fixed value $m = -0.11 < m_h$. Equilibrium point is unstable focus and there is no limit cycles. (b) Fixed value $m = -0.07 > m_h$. Unstable limit cycle around stable interior equilibrium point.*

- Fix parameter values $a = 5$, $b = c = 0.1$. Threshold value is $m_h = -0.173048$ at which system (9) has an equilibrium point $E_h(0.261946, 0.261946)$ with eigenvalues $\lambda_{1,2} = \pm0.22836i$. First Lyapunov coefficient at equilibrium point E_h for these parameter values is equal to $\ell_1 = -1.08075 < 0$. Therefore, supercritical Hopf bifurcation occurs around E_h. For fixed value $m = -0.25 < m_h$, system (9) has one interior equilibrium point $E_3(0.288044, 0.288044)$. Eigenvalues corresponding to the equilibrium point E_3 are $\lambda_{1,2} = -0.010279 \pm 0.25618i$, meaning E_3 is locally asymptotically stable focus, depicted on Figure 9-(a). As m increases above it's threshold value m_h, $m = -0.15 > m_h$, $E_3(0.253132, 0.253132)$ becomes unstable focus, while stable limit cycle appears around it, as shown on Figure 9-(b).
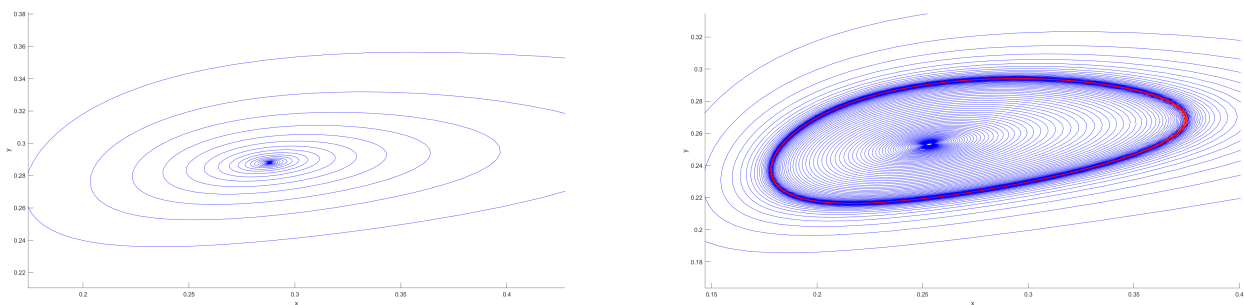
Figure 9: SUPERCRITICAL HOPF BIFURCATION IN THE CASE OF WEAK ALLEE EFFECT: *Phase portraits of the system (9) for fixed values of parameters $a = 5$, $b = c = 0.1$. The system exhibits supercritical Hopf-bifurcations at $m_h = -0.173048$. (a) Fixed value $m = -0.25 < m_h$. Equilibrium point is locally asymptotically stable focus and there is no limit cycles. (b) Fixed value $m = -0.15 > m_h$. Stable limit cycle around unstable interior equilibrium point.*

3.3. Generalized Hopf bifurcation

The fact that system (9) undergoes both supercritical and subcritical Hopf bifurcation indicates existence of generalized Hopf bifurcation at the interior equilibrium point E_h. The system exhibits a Bautin or

generalised Hopf bifurcation at the interior equilibrium point E_h when the first Lyapunov number at the Hopf bifurcating threshold m_h is zero. Two limit cycles are generated from such a bifurcation by perturbing the parameters m and a in the neighborhood of the parameters critical values m_{gh} and a_{gh}. Although analytically, conditions for this bifurcation are difficult to produce for the observed system, due to its complicated nature, numerically by fixing the parameters b and c, it can be verified that the system exhibits generalized Hopf bifurcation around equilibrium E_h for bifurcation parameter values (a, m) near (a_{gh}, m_{gh}). Direction of the generalized Hopf bifurcation, that is the stability of the two limit cycles is determined by the sign of the second Lyapunov coefficient ℓ_2. If $\ell_2 > 0$, system undergoes subcritical generalized Hopf bifurcation, meaning that equilibrium E_h is an unstable weak focus of multiplicity two and two limit cycles can coexist around it, inner one being stable, outer one unstable. If $\ell_2 < 0$, system undergoes supercritical generalized Hopf bifurcation, meaning that equilibrium E_h is locally asymptotically stable weak focus of multiplicity two and two limit cycles can coexist around it, inner limit cycle will be unstable, while outer one is stable.

- Fix the values $b = c = 0.15$. Critical bifurcation values are $a_{gh} = 0.707731$ and $m_{gh} = 0.224074$. For these values, system (9) has two interior equilibrium points, saddle $E_4(0.322451, 0.322451)$ and a weak focus $E_5(0.48295, 0.48295)$. Numerical calculations show that for the equilibrium point E_5, the first Lyapunov coefficient is $\ell_1 = 0$, while the value of the second Lyapunov coefficient is $\ell_2 = 8.20144 > 0$. For values of parameters $a = 0.7222 > a_{gh}$ and $m = 0.2199 < m_{gh}$, equilibrium point $E_3(0.480079, 0.480079)$ is unstable focus. Two limit cycles exist around E_5, inner one being stable, while outer one is unstable. Bifurcation diagram of the system is shown on Figure 10.

- Fix the values $b = c = 0.102$. Critical bifurcation values are $a_{gh} = 7.582835$ and $m_{gh} = -0.0491589$. For these values, system (9) has only one interior equilibrium point, weak focus $E_3(0.151578, 0.151578)$. Numerical calculations show that, for equilibrium point E_3, the first Lyapunov coefficient is $\ell_1 = 0$. The value of the second Lyapunov coefficient is $\ell_2 = -1096.76 < 0$. For values of parameters $a = 6.97 < a_{gh}$ and $m = -0.0197 > m_{gh}$, equilibrium point $E_3(0.142804, 0.142804)$ is locally asymptotically stable focus. Two limit cycles exist around E_3, inner one being unstable while outer one is stable.

It is important to mention that system may not exhibit the generalized Hopf bifurcation under certain conditions. For example, for fixed values of parameters $b = c = 0.182$, first Lyapunov coefficient is always positive, meaning that only subcritical Hopf bifurcation can occur.
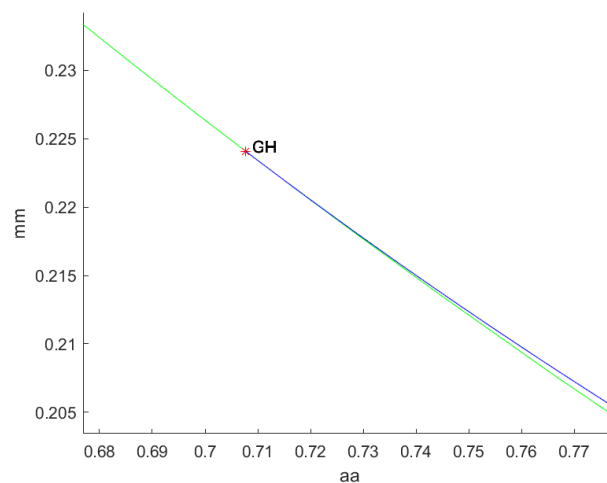
Figure 10: *Bifurcation diagram of generalized Hopf bifurcation for fixed values of parameters $b = c = 0.15$. Curve of Hopf bifurcation is colored green, while the curve of saddle-node bifurcation of limit cycles is colored blue.*

3.4. Bogdanov-Takens bifurcation

Existence of both saddle-node bifurcation and Hopf bifurcation suggests that system (9) might undergo Bogdanov-Takens bifurcation, introduced by Bogdanov [6, 7] and Takens [26]. In fact, if two interior equilibrium appears through the saddle–node bifurcation and one of them changes stability via Hopf bifurcation, Bogdanov-Takens bifurcation of codimension 2 might occur at an interior equilibrium point denoted by $E_{bt}(x_{bt}, y_{bt})$, where $y_{bt} = bx_{bt}/c$. Choosing a and m as bifurcation parameters, BT bifurcation threshold values are a_{bt}, m_{bt}, that is $det(J_{BT})\big|_{(a,m)=(a_{bt},m_{bt})} = 0$, $tr(J_{BT})\big|_{(a,m)=(a_{bt},m_{bt})} = 0$, $J_{BT} = J(x_{bt}, y_{bt})$, so that the Jacobian matrix at E_{bt} has a zero eigenvalue with multiplicity two. For $(a, m) = (a_{bt}, m_{bt})$ both saddle-node and Hopf bifurcation collide with each other and the instantaneous equilibrium point becomes a cusp of co-dimension two.

Due to the complexity of the expressions it is difficult to find explicit parametric conditions for a_{bt} and m_{bt}, but numerically it can be verified that the system exhibits Bogdanov–Takens (BT) bifurcation. Next theorem gives conditions under which a unique interior equilibrium E_{bt} is a cusp of codimension two (for the proof see Appendix A.1).

Theorem 3.3. *For the value of parameters $(a, m) = (a_{bt}, m_{bt})$, system (9) has interior equilibrium $E_{bt}(x_{bt}, y_{bt})$ which is a cusp point of codimension 2 (a Bogdanov–Takens singularity) if and only if $s_1 s_2 \neq 0$, where s_1 and s_2 are given by*

$$s_1 = \frac{c\left(b^3 x_{bt}^5 - 2c^2 x_{bt}(1 - 3x_{bt} + 3x_{bt}^2) - 3bck_1 - b^2 x_{bt}^2 k_2\right)}{x_{bt}(2x_{bt} - 1)(c + bx_{bt}^2)(2c + bx_{bt}^2)}, \quad s_2 = \frac{2c\left(b^3 x_{bt}^5 - 2c^2 x_{bt}(1 - 3x_{bt} + 3x_{bt}^2) + bck_3 - b^2 x_{bt}^2 k_2\right)}{bx_{bt}(2x_{bt} - 1)(c + bx_{bt}^2)(2c + bx_{bt}^2)},$$

$$k_1 = c(x_{bt} - 1) + x_{bt}^3 + 3x_{bt}^4(x_{bt} - 1), \quad k_2 = c(1 - 6x_{bt}) + x_{bt}^3 + 3x_{bt}^4(x_{bt} - 1), \quad k_3 = c(1 + x_{bt}) - 3x_{bt}^3(1 - 3x_{bt} + 3x_{bt}^2).$$

(26)

Also, in Appendix A.2 the nondegeneracy condition of the Bogdanov-Takens (BT) bifurcation is proved, using procedure described by Kuznetsov [14]. By employing a series of change of coordinates in a small neighborhood of the origin, the system (27) is reduced to the normal form of a Bogdanov-Takens bifurcation (see (33)), in which the sign of S determines if the BT bifurcation is supercritical or subcritical.

4. Numerical simulations

To show the locations of bifurcation curves SN, H and HL, and sub-regions in the parametric plane they separate, we utilize numerical simulation. We fix the parameters b and c while we vary parameters a and m to generate bifurcation curves. Bifurcation diagram is shown on Figure 11. Saddle-node bifurcation curve SN is represented with blue curve, Hopf bifurcation curve H is represented with green curve and homoclinic bifrucation curve HL is represented with red curve. We find that curves H and SN intersect each other at two points. Namely, this means that there are two points in parameter space at which Bogdanov-Takens bifurcation occurs. Bifurcation curve HL emerges from one BT point and intersects SN curve in other BT point. On H curve, there exists a generalized Hopf bifurcation point, which is denoted with GH. There is one more bifurcation curve originating at the point GH, denoted as curve T, at which a saddle-node bifurcation of limit cycles take place.

These bifurcation curves dissect the parameter space into six regions, labeled from **I** to **VI**. The dynamics of the system (9), as well as number of interior equilibria and limit cycles, change as parameters a and m move through different regions. In region **I**, system (9) has no interior equilibrium points, as shown on Figure 12-(a). From region **I**, parameters can enter either to region **II** or to region **VI**.

(i) Moving from region **I** to region **VI**, through the saddle-node bifurcation, two interior equilibria appear, E_4 which is saddle and E_5 which is locally asymptotically stable focus, as shown on Figure 12-(f).

(ii) Moving from region **I** to region **II**, through the saddle-node bifurcation, two interior equilibria appear, E_4 which is saddle and E_5 which is an unstable focus. Phase portrait is shown on Figure 12-(b). From region **II**, parameters can enter three different regions: either to the region **IV**, through part of the H curve, between left BT point and GH point, or to the region **III** through curve T, or to the region **V** through HL curve.

(ii-1) From region **II** to region **IV** through subcritical Hopf bifurcation, unstable focus E_5 becomes locally asymptotically stable focus surrounded by an unstable limit cycle, as shown on Figure 12-(d). These limit cycle expand as the parameters approach the homoclinic bifurcation curve, at which the system has a homoclinic orbit at the saddle point E_4. When the parameters enter region **VI** limit cycle no longer exists, while two interior equilibria exists, a saddle point E_4 and a locally asymptotically stable focus E_5.

(ii-2) As parameters pass from region **II** to region **III**, stability of two interior equilibrium points does not change, however through saddle-node bifurcation of limit cycles two limit cycles appear around unstable focus E_5, inner limit cycle is stable and outer is unstable, as shown on Figure 12-(c). From region **III**, parameters can enter either to region **IV** or to region **V**.

(ii-2-a) If parameter values move from region **III** to region **IV**, the stability of E_5 is changed through supercritical Hopf bifurcation and it becomes locally asymptotically stable focus surrounded by an unstable limit cycle, while inner stable limit cycle disappears.

(ii-2-b) If parameter values move from region **III** to region **V**, outer unstable limit cycle disappears through homoclinic bifurcation, while the stability of the unstable inner equilibria E_5 and inner stable limit cycle do not change. Transition from **V** to **VI** results in appearance of supercritical Hopf bifurcation around E_5, which changes its stability and limit cycle disappears.

(ii-3) In the region **V** system has two interior equilibria, saddle point and unstable focus surrounded by stable limit cycle, which expand as the parameter approach the homoclinic bifurcation curve *HL*, between regions **V** and **II**. At *HL* curve the system has a homoclinic orbit at the saddle point E_4, so that in the region **II** limit cycle disappears, while the two equilibrium points remain and do not change the stability.
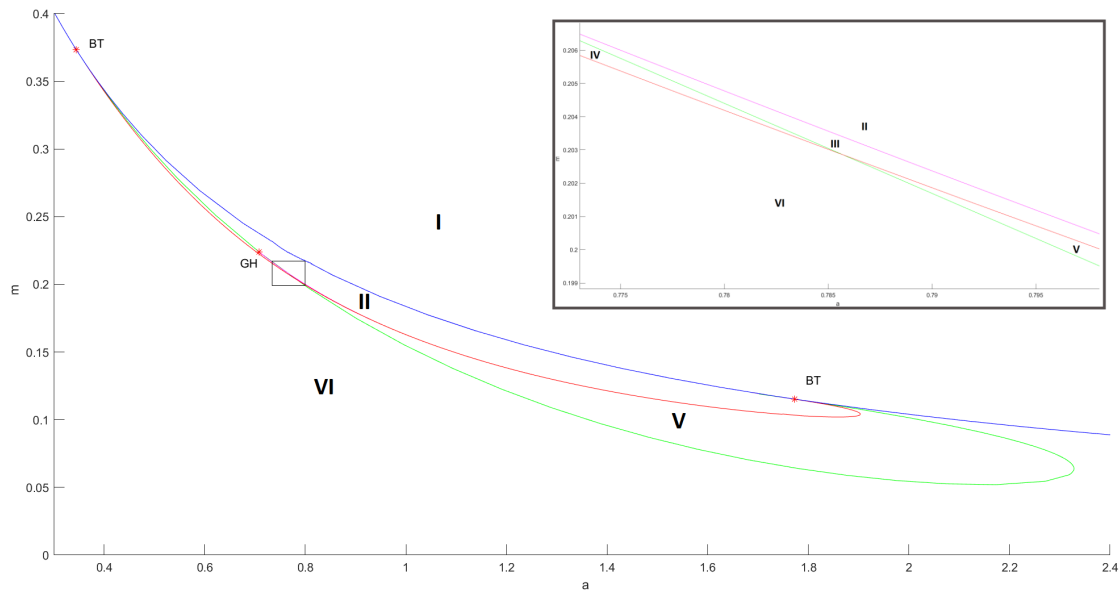
Figure 11: *Bifurcation diagram of the system* (9) *in am–plane for fixed values of parameters b = c = 0.15. Saddle-node bifurcation curve SN (blue), Hopf bifurcation curve H (green), homoclinic bifurcation curve HL (red). Two Bogdanov-Takens points labeled with BT are located at the intersection of the curves curves H and SN, one generalized Hopf bifurcation point GH. Magenta curve that originating at the point GH represents bifurcation curve T. This curve is significant only until its intersection with HL red curve. These curves divide the parametric space into six different regions, labeled by roman numerals **I** to **VI**.*

(a) Region (I)

(b) Region (II)

(c) Region (III)

(d) Region (IV)

(e) Region (V)

(f) Region (VI)
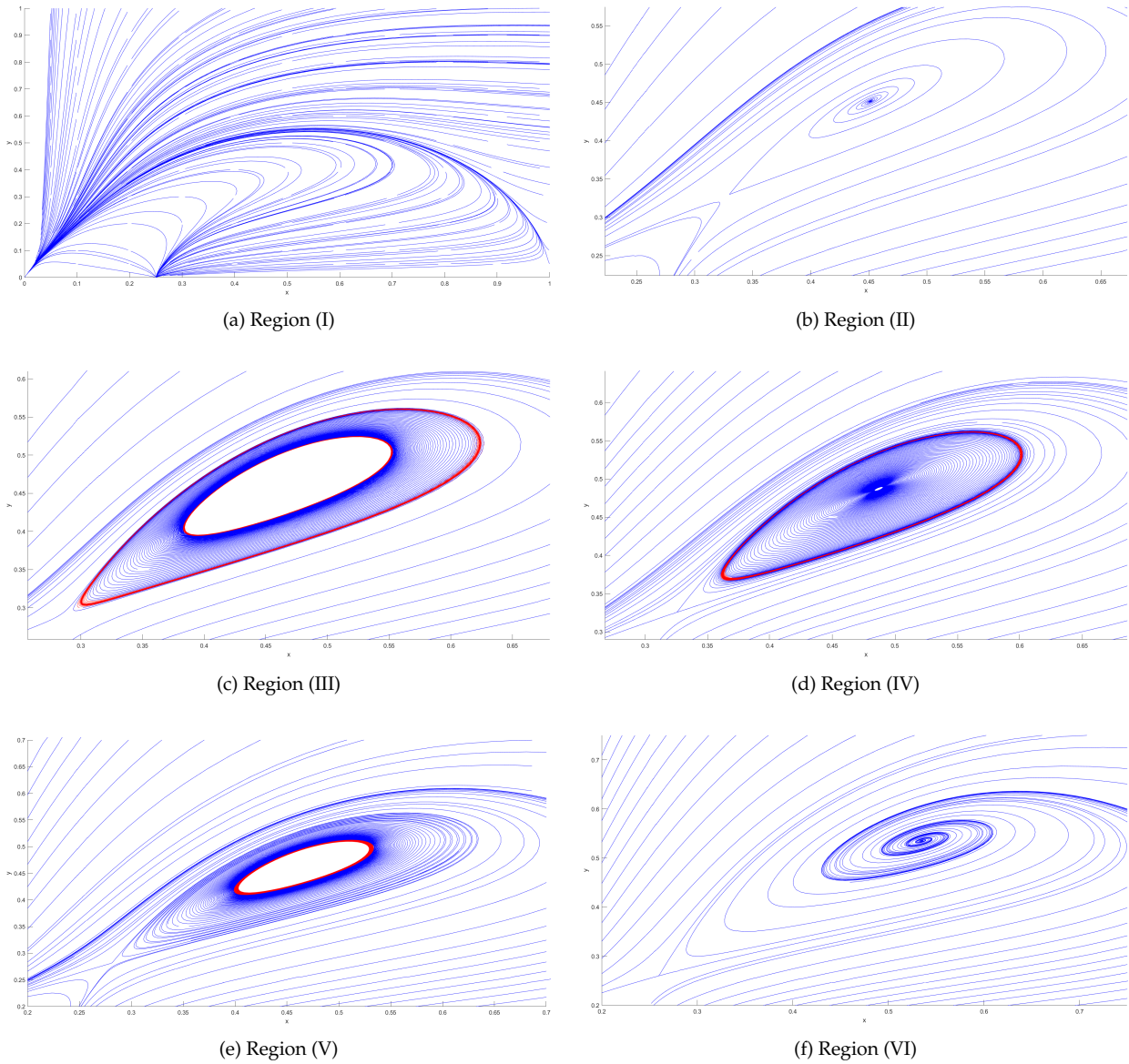
Figure 12: *Figure illustrates phase portraits of the system* (9) *for different regions of Figure 11, for fixed parameters* $b = c = 0.15$ *and varied parameters a and m.*

a) $(a, m) = (1, 0.25) \in I$: *there aren't any interior equilibria, and origin is global attractor.*

b) $(a, m) = (0.75, 0.22) \in II$: *two interior equilibria exist, saddle point* E_4 *and unstable focus* E_5. *No limit cycle surrounds equilibrium point* E_5.

c) $(a, m) = (0.786, 0.203) \in III$: *two interior equilibria exist, saddle point* E_4 *and unstable focus* E_5 *surrounded by two limit cycles, inner one being stable and outer one unstable.*

d) $(a, m) = (0.697, 0.2265) \in IV$: *two interior equilibria exist, saddle point* E_4 *and locally asymptotically stable focus* E_5 *surrounded by an unstable limit cycle.*

e) $(a, m) = (0.797, 0.2) \in V$: *two interior equilibria exist, saddle point* E_4 *and unstable focus* E_5 *surrounded by a stable limit cycle.*

f) $(a, m) = (0.7, 0.2) \in VI$: *two equilibrium points exist, saddle point* E_4 *and locally asymptotically stable focus* E_5. *No limit cycle surrounds equilibrium point* E_5.

Numerical simulations show another interesting dynamics. For certain values of parameters b and c, it is possible for three generalized Hopf bifurcation points to exist. Figure 13 show bifurcation diagram of system (9) for fixed parameter values $b = c = 0.102$. The additional two bifurcation points GH lie on the Hopf bifurcation curve H and are connected with bifurcation curve T, represented with magenta colored curve. Now, before entering region **V** from region **VI**, parameters must pass through region **VII**, bounded with bifurcation curves between two GH points that corresponds to the saddle-node bifurcation of limit cycles and Hopf bifurcation curve. In this region, equilibrium point E_5 is locally asymptotically stable focus, while two limit cycles surround it, inner limit cycle being unstable and outer being stable. Through subcritical Hopf bifurcation, which occurs as parameters pass into region **V**, E_5 becomes unstable focus, the inner unstable limit cycle disappears, while the stable outer limit cycle remains surrounding E_5.
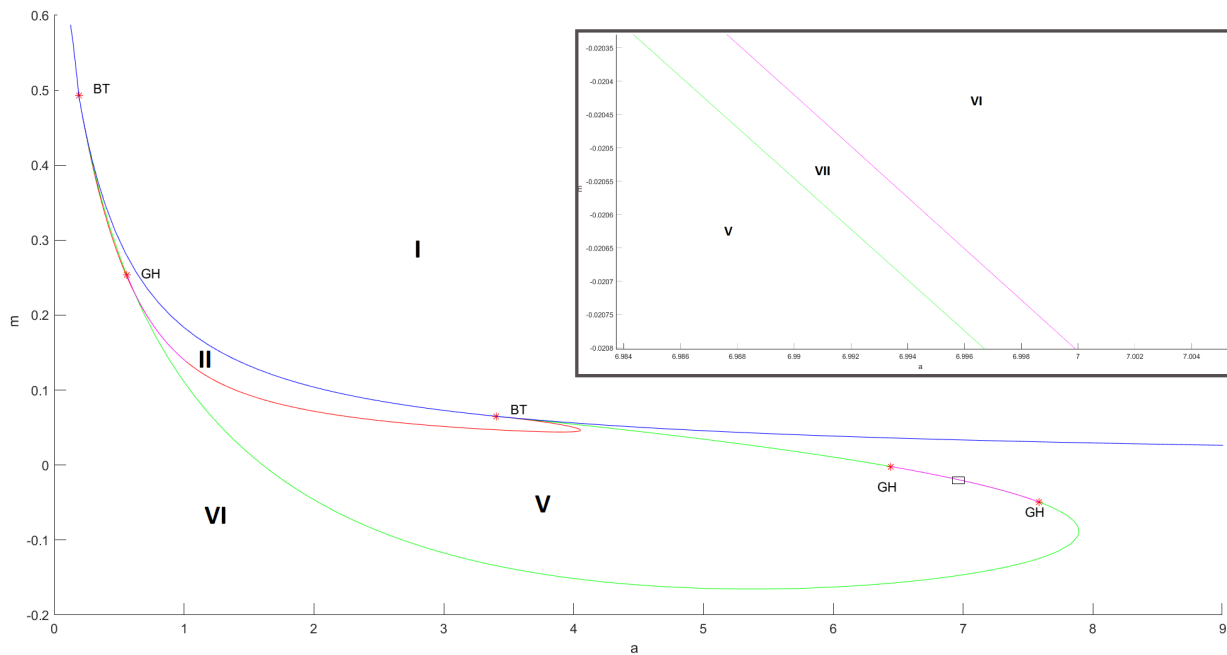
Figure 13: *Bifurcation diagram of the system* (9) *for fixed values of parameters* $b = c = 0.102$. *Saddle-node bifurcation curve SN (blue), Hopf bifurcation curve H (green), homoclinic bifurcation curve HL (red), bifurcation curves T (magenta).*

As it was mentioned earlier when we discussed existence of generalized Hopf bifurcation, under certain conditions only subcritical Hopf bifurcation can exists. Bifurcation diagram of system (9) for parameter values $b = c = 0.182$ is shown on Figure 14. In this case, bifurcation curves dissect parameter space into four regions, labeled **I** to **IV**. In region **I**, system (9) has no interior equilibria. From region **I**, parameters can enter either to region **II** or to region **IV**.

(i) Moving from region **I** to region **IV**, through the saddle-node bifurcation, two interior equilibria appear, E_4 which is saddle and E_5 which is locally asymptotically stable focus.

(ii) Moving from region **I** to region **II**, two interior equilibria appear, E_4 which is saddle and E_5 which is unstable focus. As parameters pass from region **II** into region **III**, subcritical Hopf bifurcation gives rise to unstable limit cycle while E_5 becomes locally asymptotically stable focus. Through homoclinic bifurcation, which occurs as parameters pass from region **III** into region **IV**, limit cycle collides with saddle E_4 and disappears, while the stability of interior equilibria doesn't change.
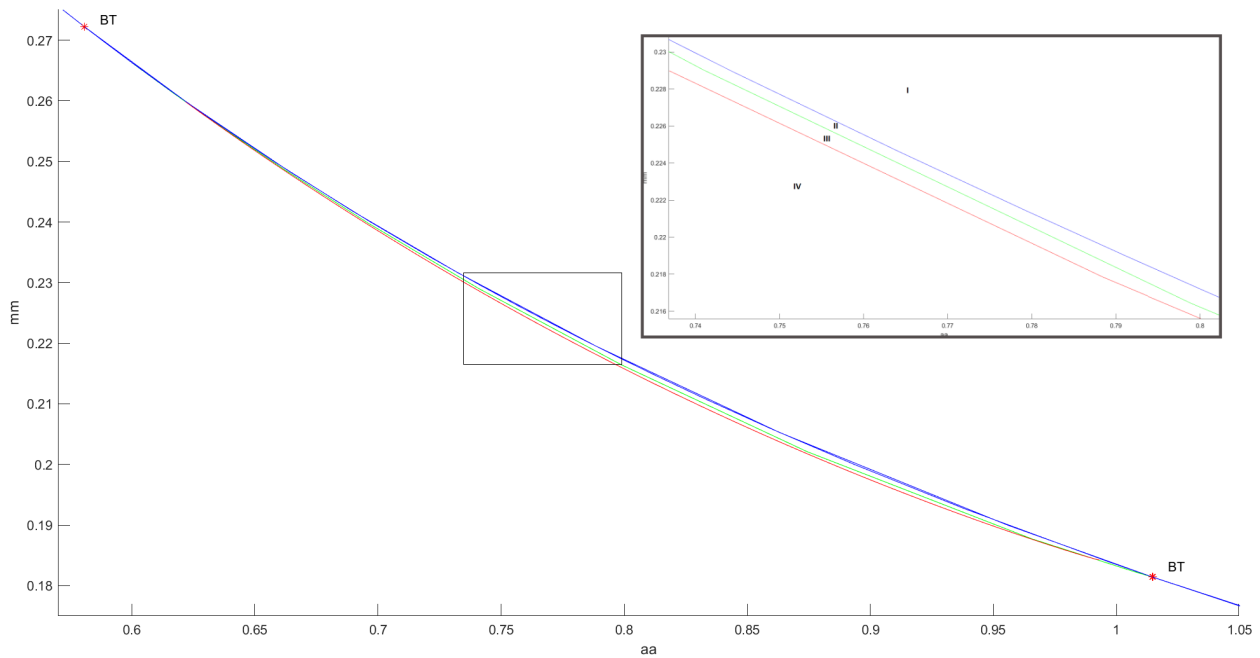
Figure 14: *Bifurcation diagram of the system* (9) *for parameter values b = c = 0.182. Saddle-node bifurcation curve SN is represented with blue curve. Hopf bifurcation curve H is represented with green curve. Homoclinic bifurcation curve HL is represented with red curve.*

5. Basins of attraction

Previously we concluded that, in the case of strong Allee effect, the system (9) can have more than one attractor. One of them is always the origin and the basin of attraction of the origin has been discussed in Section 1.2.3. The system (9) may have two more attractors, either a stable limit cycles or locally asymptotically stable equilibria. The basin of attraction $\mathcal{B}(\gamma)$ of the stable limit cycle γ is the set of all points in phase space that converge to this limit cycle in forward time. In this section we discuss the basins of attraction of all possible attractors, as we will determine the existence of separatrices in the phase plane separating basins of attraction related to periodic co-existence and extinction of both predator and prey population.

We proved that equilibrium point E_4 is always a saddle point. The stable manifold of saddle point E_4, $W^s(E_4)$, often acts as separatrix curve between basins of attraction of two attractors. Let $W^s_{\searrow}(E_4)$ be the branch of the stable manifold of saddle point E_4 that approaches E_4 from top right, while $W^s_{\nearrow}(E_4)$ is the branch that approaches E_4 from bottom left. Similarly, $W^u_{\nearrow}(E_4)$ denotes the branch of the unstable manifold of saddle point E_4 that escapes E_4 towards top right, while $W^u_{\swarrow}(E_4)$ is the branch that escapes toward bottom left. We also observe the behaviour of the branch of the unstable manifold of the saddle point E_2 that belongs to the open firts quadrant, denoted with $W^u(E_2)$. Moreover, we can deduce that there are always two heteroclinic connections: $\mathcal{H}_{14}$ between E_1 and E_4, which is a subset of $W^u(E_1) \cap W^s_{\nearrow}(E_4)$, and $\mathcal{H}_{12}$ between E_1 and E_2, which is a subset of $W^u(E_1) \cap W^s(E_2)$. Also, there is an orbit $\mathcal{H}_{40}$ which is a subset of $W^u_{\swarrow}(E_4)$ and approaches the origin. These orbits are marked with green line in all images bellow.

Depending on the value of parameters, when the bifurcation diagram is shown in Figure 11, there are four possible cases that can occur, in which system (9) has two attractors - either the origin and the stable interior equilibrium or the origin and the stable limit cycle. Basins of attraction are shown on Figures 15, 16, 17 and 18. However, in the case the system has three *GH* points, that is for the bifurcation diagram shown in Figure 13, system (9) may have three attractors : the origin, the stable interior equilibrium and the stable limit cycle and possible basins of attraction are shown on Figure 19. In each of this figures basin

of attraction $\mathcal{B}(\mathbf{0})$ is colored in yellow, basin of attraction of the stable interior equilibrium is colored in blue and basin of attraction of the stable limit cycle is colored in green. Therefore, solutions with initial values in yellow colored area will be driven to the extinction of both species, solutions with initial values in blue colored area will tend to the locally asymptotically stable focus, corresponding to the stable periodic coexistence, while solutions with initial values in green colored area will tend to the stable limit cycle, that is the prey and predator will oscillate periodically.

1. Let the equilibrium point E_5 be a locally asymptotically stable focus with an unstable limit cycle around it (parameters $(a, m) \in \mathbf{IV}$ at Figure 11). In this case an unstable limit cycle γ serves as separatrix curve between basins of attraction $\mathcal{B}(\mathbf{0})$ (yellow) and $\mathcal{B}(E_5)$ (blue), shown on Figure 15. Notice that the unstable manifold $W^u(E_2)$ tends to the origin as $t \to +\infty$ (black line at Figure 15), while the stable manifold $W^s_\swarrow(E_4)$ tends to the unstable limit cycle γ as $t \to -\infty$ (red line at Figure 15).
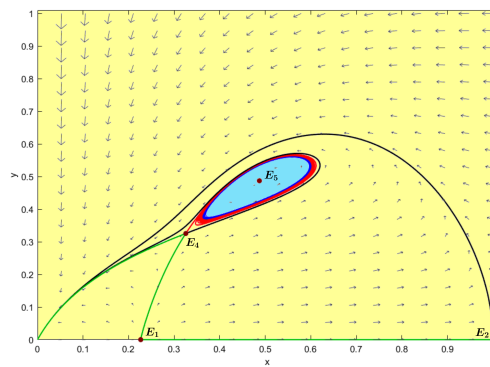
Figure 15: *Basins of attraction $\mathcal{B}(\mathbf{0})$ (yellow) and $\mathcal{B}(E_5)$ (blue), when E_5 is locally asymptotically stable focus surrounded by an unstable limit cycle γ (blue). Green lines are a heteroclinic connection $\mathcal{H}_{14}$ between E_1 and E_4, the orbit $\mathcal{H}_{40}$ which is a subset of $W^u_\swarrow(E_4)$ and approaches the origin. Red line is the stable manifold $W^s_\swarrow(E_4)$ tending to the unstable limit cycle γ as $t \to -\infty$.*

| (a) | (b) | (c) |
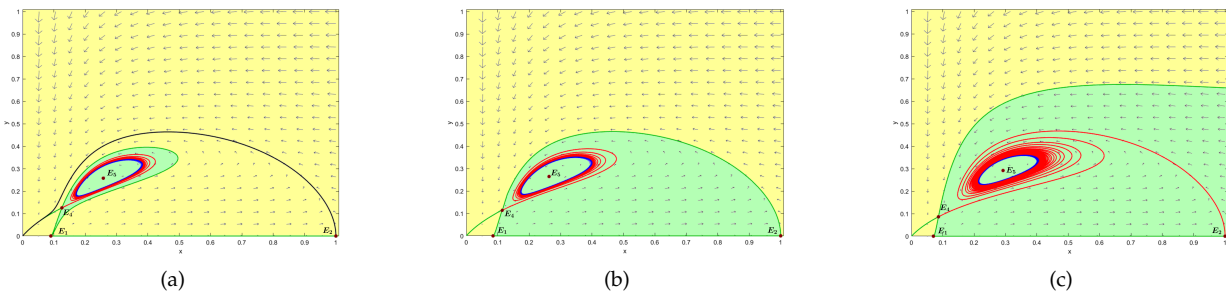
Figure 16: *Basins of attraction $\mathcal{B}(\mathbf{0})$ (yellow) and $\mathcal{B}(\gamma)$ (green), when E_5 is an unstable focus surrounded by a stable limit cycle γ (blue). (a) Green lines depict heteroclinic connections $\mathcal{H}_{14}$ and $\widehat{\mathcal{H}_{14}}$, which separate the two basins of attraction. (b) Green lines depict heteroclinic connections $\mathcal{H}_{14}$ and $\mathcal{H}_{24}$, which separate the two basins of attraction. (c) Green lines depict heteroclinic connections $\mathcal{H}_{14}$ and the stable manifold $W^s_\swarrow(E_4)$, which separate the two basins of attraction.*

2. Let the equilibrium point E_5 be an unstable focus with a stable limit cycle γ around it (parameters $(a, m) \in \mathbf{V}$ at Figure 11). To determine basins of attraction $\mathcal{B}(\mathbf{0})$ (yellow) and $\mathcal{B}(\gamma)$ (green), shown on Figure 16 we distinguish three subcases, depending on the behavior of the branch $W^u(E_2)$:

(2-a) It may happen that the unstable manifold $W^u(E_2)$ tends to the origin as $t \to +\infty$. In that case, there is one more heteroclinic connection $\widehat{\mathcal{H}_{14}}$ between E_1 and E_4, which is a subset of $W^u(E_1) \cap W^s_{\nearrow}(E_4)$. This heteroclinic orbit together with the heteroclinic connection $\mathcal{H}_{14}$ separate the two basins of attraction, as shown on Figure 16-(a).

(2-b) It may happen that there is one more heteroclinic connection $\mathcal{H}_{24}$ between E_2 and E_4, which is a subset of $W^u(E_2) \cap W^s_{\nearrow}(E_4)$. This heteroclinic orbit together with the heteroclinic connection $\mathcal{H}_{14}$ separates the two basins of attraction, as shown on Figure 16-(b).

(2-c) It may happen that the unstable manifold $W^u(E_2)$ tends to the stable limit cycle γ as $t \to +\infty$. In the case the stable manifold $W^s_{\nearrow}(E_4)$ together with the heteroclinic connection $\mathcal{H}_{14}$ serve as separatrix curves between two basins of attraction, as shown on Figure 16-(c).

3. Equilibrium point E_5 is unstable focus with two limit cycles around it, inner one γ_1 being stable and outer one γ_2 being unstable (parameters $(a, m) \in$ **III** at Figure 11). In this case the outer unstable limit cycle γ_2 serves as the separatrix curve between two basins of attraction $\mathcal{B}(\mathbf{0})$ (yellow) and $\mathcal{B}(\gamma_1)$ (green), shown on Figure 17.
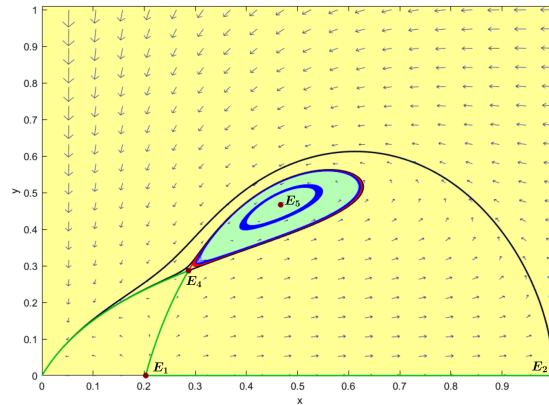
Figure 17: *Basins of attraction $\mathcal{B}(\mathbf{0})$ (yellow) and $\mathcal{B}(\gamma_1)$ (green), when E_5 is unstable focus surrounded by two limit cycles, inner one γ_1 being stable and outer one γ_2 being unstable. Limit cycles are colored with blue color.*

4. Equilibrium point E_5 is locally asymptotically stable focus with no limit cycles around it (parameters $(a, m) \in$ **VI** at Figure 11). We have two basins of attraction $\mathcal{B}(\mathbf{0})$ (yellow) and $\mathcal{B}(E_5)$ (blue), shown on Figure 18. Similarly as in the case 2., to determine the separtices between $\mathcal{B}(\mathbf{0})$ and $\mathcal{B}(E_5)$, we distinguish three subcases, depending on the behavior of the branch $W^u(E_2)$:

(4-a) It may happen that the unstable manifold $W^u(E_2)$ tends to the origin as $t \to +\infty$. In that case, heteroclinic connection $\widehat{\mathcal{H}_{14}}$ between E_1 and E_4 together with the heteroclinic connection $\mathcal{H}_{14}$ separate the two basins of attraction, as shown on Figure 18-(a).

(4-b) It may happen that there is one more heteroclinic connection $\mathcal{H}_{24}$ between E_2 and E_4, which together with the heteroclinic connection $\mathcal{H}_{14}$ separates the two basins of attraction, as shown on Figure 18-(b).

(4-c) It may happen that the unstable manifold $W^u(E_2)$ tends to the stable equilibrium E_5 as $t \to +\infty$, in which case the stable manifold $W^s_{\nearrow}(E_4)$ together with the heteroclinic connection $\mathcal{H}_{14}$ serve as separatrix curves between two basins of attraction, as shown on Figure 18-(c).

(a)   (b)   (c)
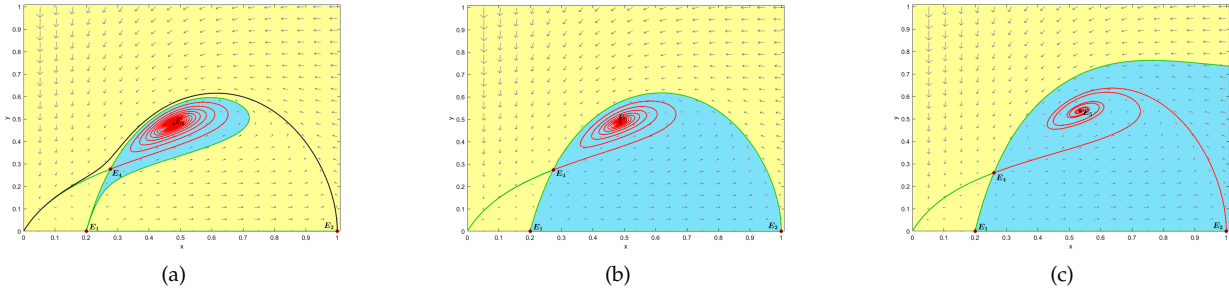
Figure 18: $\mathcal{B}(\mathbf{0})$ (yellow) and $\mathcal{B}(E_5)$ (blue), when E_5 is a locally asymptotically stable focus with no limit cycles around it. (a) Green lines depict heteroclinic connections $\mathcal{H}_{14}$ and $\widehat{\mathcal{H}_{14}}$, which separate the two basins of attraction $\mathcal{B}(\mathbf{0})$ and $\mathcal{B}(E_5)$. (b) Green lines depict heteroclinic connections $\mathcal{H}_{14}$ and $\mathcal{H}_{24}$, which separate the two basins of attraction $\mathcal{B}(\mathbf{0})$ and $\mathcal{B}(E_5)$. (c) Green lines depict heteroclinic connections $\mathcal{H}_{14}$ and the stable manifold $W^s_{\swarrow}(E_4)$, which separate the two basins of attraction $\mathcal{B}(\mathbf{0})$ and $\mathcal{B}(E_5)$.

5. Equilibrium point E_5 is locally asymptotically stable focus with two limit cycles around it, inner one γ_1 being unstable and outer one γ_2 is a stable (parameters $(a, m) \in$ **VII** at Figure 13). We have now three basins of attraction $\mathcal{B}(\mathbf{0})$ (yellow), $\mathcal{B}(\gamma_2)$ (green) and $\mathcal{B}(E_5)$ (blue), shown on Figure 19. In this case the inner unstable limit cycle γ_1 serves as the separatrix curve between two basins of attraction $\mathcal{B}(\gamma_2)$ and $\mathcal{B}(E_5)$. To determine the separtices between $\mathcal{B}(\mathbf{0})$ and $\mathcal{B}(\gamma_2)$, we distinguish three subcases, depending on the behavior of the branch $W^u(E_2)$:

(5-a) It may happen that the unstable manifold $W^u(E_2)$ tends to the origin as $t \to +\infty$. In that case, there is one more heteroclinic connection $\widehat{\mathcal{H}_{14}}$ between E_1 and E_4, which is a subset of $W^u(E_1) \cap W^s_{\swarrow}(E_4)$. This heteroclinic orbit together with the heteroclinic connection $\mathcal{H}_{14}$ separate the two basins of attraction $\mathcal{B}(\mathbf{0})$ and $\mathcal{B}(\gamma_2)$, as shown on Figure 19-(a).

(5-b) It may happen that there is one more heteroclinic connection $\mathcal{H}_{24}$ between E_2 and E_4, which is a subset of $W^u(E_2) \cap W^s_{\swarrow}(E_4)$. This heteroclinic orbit together with the heteroclinic connection $\mathcal{H}_{14}$ separates the two basins of attraction $\mathcal{B}(\mathbf{0})$ and $\mathcal{B}(\gamma_2)$, as shown on Figure 19-(b).

(5-c) It may happen that the unstable manifold $W^u(E_2)$ tends to the stable limit cycle γ_2 as $t \to +\infty$. In this case the stable manifold $W^s_{\swarrow}(E_4)$ together with the heteroclinic connection $\mathcal{H}_{14}$ serve as separatrix curves between two basins of attraction $\mathcal{B}(\mathbf{0})$ and $\mathcal{B}(\gamma_2)$, as shown on Figure 19-(c).

(a)   (b)   (c)
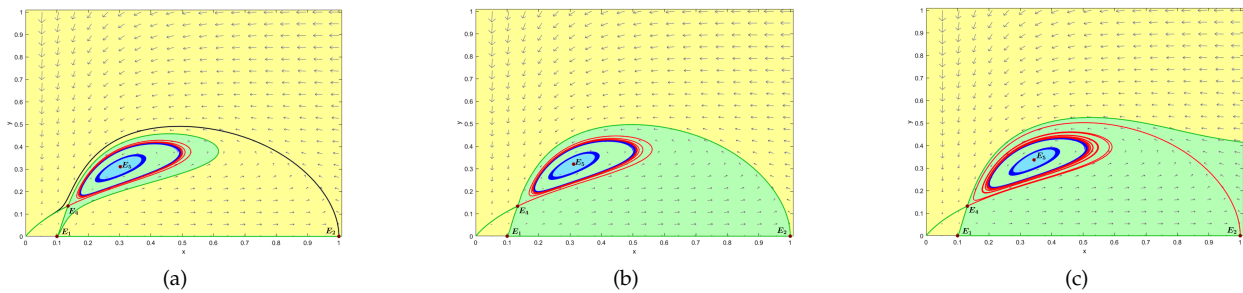
Figure 19: $\mathcal{B}(\mathbf{0})$ (yellow), $\mathcal{B}(\gamma_2)$ (green) and $\mathcal{B}(E_5)$ (blue), when E_5 is a stable focus surrounded by two limit cycles, inner one γ_1 being unstable and outer one γ_2 is stable. The inner unstable limit cycle γ_1 serves as the separatrix curve between two basins of attraction $\mathcal{B}(\gamma_2)$ and $\mathcal{B}(E_5)$. (a) Green lines depict heteroclinic connections $\mathcal{H}_{14}$ and $\widehat{\mathcal{H}_{14}}$, which separate the two basins of attraction $\mathcal{B}(\mathbf{0})$ and $\mathcal{B}(\gamma_2)$. (b) Green lines depict heteroclinic connections $\mathcal{H}_{14}$ and $\mathcal{H}_{24}$, which separate the two basins of attraction $\mathcal{B}(\mathbf{0})$ and $\mathcal{B}(\gamma_2)$. (c) Green lines depict heteroclinic connections $\mathcal{H}_{14}$ and the stable manifold $W^s_{\swarrow}(E_4)$, which separate the two basins of attraction $\mathcal{B}(\mathbf{0})$ and $\mathcal{B}(\gamma_2)$.

6. Conclusion

In this paper, we studied the dynamics and bifurcations of the Leslie-Gower predator-prey system with increasing functional response proposed in [8] and Allee effect on prey. This system was first reduced to a system with only four parameters using proper parameter scaling. The proposed model is shown biologically well-posed in the sense that any positive solution starts in the first quadrant remains non-negative and ends up in the invariant region Φ.

We compare the dynamic of the model with the weak Allee effect (WAE) and with a strong Allee effect (SAE) relative to the existence and stability of equilibrium points, bifurcation and multiple attractors.

Existence and stability of equilibria: First, all possible equilibria and their local stability are explored. Using the blow-up method (described in [11]) to desingularize the origin, the dynamics of the system near origin is determined.

(a) In the case of WAE, it was shown: (a) system always has a unique axial equilibrium $E_2(1,0)$ which is a hyperbolic saddle; (b) for some values of parameters system has the unique interior equilibrium E_3 whose local stability changes depending on the parameters; (c) the origin is a local repeller, so populations will always persist.

(b) In the case of SAE, it was shown: (a) system always has two axial equilibriums $E_1(m,0)$ which is an unstable hyperbolic node and $E_2(1,0)$ which is a hyperbolic saddle; (b) for some values of parameters system has at most two interior equilibriums E_4 and E_5, one of them being always a saddle point, while local stability of the other one changes depending on the parameters; (c) the origin is a local attractor, so the extinction of both species is possible.

Bifurcation: Next, bifurcations of the system were studied. Since we wanted to see how the Allee effect in prey and the increasing functional response affect the system dynamics, we have constructed a two parametric bifurcation diagram taking m and a as the two bifurcation parameters. It was shown that regardless of the strength of the Allee effect, both subcritical and supercritical Hopf bifurcation occur, by choosing m as the bifurcation parameter, producing either an unstable limit cycle or a stable limit cycle. Also, by choosing a and m as the bifurcation parameters, generalized Hopf bifurcation occurs, producing two limit cycles. On the other hand, BT bifurcation of codimension 2 can occur only when prey population is under the influence of strong Allee effect. Existence of multiple codimension two bifurcation points implies the existence of codimension 3 bifurcation points, however their existence wasn't studied.

More precisely:

(a) In the case of WAE system can only have unique equilibrium point E_3 at the interior of the first quadrant. The unique interior equilibrium point E_3 is either locally asymptotically stable or changes its stability through both subcritical and supercritical Hopf bifurcation. Moreover, it was shown through numerical simulation that in a small neighborhood of the unique interior equilibrium point E_3, system undergoes supercritical generalized Hopf bifurcation and E_3 is either a locally asymptotic stable or unstable and surrounded by a stable limit cycle or locally asymptotic stable surrounded by an unstable limit cycle which is surrounded by a stable limit cycle and two limit cycles disappear through saddle-node bifurcation of limit cycles. Generalized Hopf bifurcation demonstrates that there is a parametric region in which the predator and prey coexist in the form of a stable interior equilibrium for any initial value. Also, there exists another region in which multiple stable coexistence occur : the predator and prey either coexist in the form of a stable interior equilibrium for all initial values lying inside the unstable limit cycle or the predator and prey coexist in the form of a stable periodic orbit for all initial values lying outside the unstable limit cycle. Therefore, for any value of parameters, there exists an attractor in the first quadrant, so that depending on values of parameters, populations will persist with either stable periodic or oscillatory periodic behavior.

(b) In the case of SAE dynamics od the model is more complicated. We observed two important differences in the dynamic of the model with SAE and with WAE. First, unlike WAE case, SAE produces BT bifurcation of codimension 2 at the interior equilibrium E_5 which is a cusp of codimension 2. In fact, there are two *BT* points, implying that system undergoes either a reppeling or an attacting BT bifurcation of codimension 2. Second, unlike WAE case which produces only supercritical generalized Hopf bifurcation, in the case of SAE the system undergoes subcritical generalized Hopf bifurcation for certain parameters

values at the interior equilibrium E_5 which is a weak focus, while for some parameters values the system undergoes both subcritical and supercritical generalized Hopf bifurcation.

Thefore, SAE gives a rise to a very rich dynamics of the model. First we give a concluding remarks with a biological implication for a bifurcation diagram on Figure 11. We have demonstrated that there exists a great possibility of the both populations going to extinction, when parameters belong to the region **I** in which there is no interior equilibria, so that the origin is a global attractor. It is clear that if the Allee effect is significantly high there is no coexistence of the population. The model has produced saddle–node bifurcations curve which confirm the appearance or disappearance of coexistence fixed points and form parametric region where unique stable coexistence fixed point appear. The significant change in the behavior of the model due to saddle–node bifurcations is evident by the transmission from region **II** to region **I** and from region **VI** to region **I**. However, existence of two BT points produce two qualitatively different saddle–node bifurcations : first from region **VI** to region **I** when the stable periodic coexistence is destroyed and all solution trajectories settle to total extinction, and the second from region **II** to region **I**, when two unstable coexistence equilibrium points are destroyed, so that such saddle-node bifurcation does not affect the existence of the internal attractor. In the first case, it is observed that at the high intensity of a, smaller values of m are necessary to destroy the appearance of the stable coexistence equilibrium point. The model has also produced Hopf bifurcation H curve at which there is one GH point. Denote left and right BT point with BT_1 and BT_2. On H curve, Hopf bifurcation is subcritical between BT_1 point and GH point, and supercritical between GH point and BT_2 point. From a ecological point of view, Hopf bifurcation indicates the oscillatory coexistence of the species. The appearance of a stable limit cycle through supercritical Hopf-bifurcation gives the oscillatory coexistence of the species. On the other hand, the unstable limit cycle arising through subcritical Hopf-bifurcation is the boundary of the basin of attraction of the stable equilibrium point. Through this bifurcation, transition from **IV** to **II** results that system loses the internal attractor. It is observed that in the small parametric region **III** the model exhibits two limit cycles, one of which is stable and around unstable interior equilibrium, and another is an unstable limit cycle surrounding the stable limit cycle. Therefore, in this parametric region the predator and prey coexist in the form of a stable periodic orbit for all initial values lying inside the unstable limit cycle. Finally, the emergence of homoclinic loop has been shown through numerical simulation when the limit cycle collides with a saddle point.

The model produces three qualitatively different homoclinic curves regarding the stability of a separatrix cycle, depending on the type of BT bifurcation:

  (i) on HL curve between regions **II** and **V** homoclinic loop Γ at a saddle E_4 surround an unstable equilibrium, creating the stable separatrix cycle $\Gamma^+ = \Gamma \cup \{E_4\}$. In this case, model exhibits bi-stability between the origin and a separatrix cycle Γ^+ and solutions with initial values inside the separatrix cycle Γ^+ converge towards this cycle, while solutions with initial values outside the separatrix cycle Γ^+ converge towards the origin;

  (ii) on HL curve between regions **IV** and **VI** homoclinic loop Γ at a saddle E_4 surround a stable equlibrium E_5, creating an unstable separatrix cycle $\Gamma^- = \Gamma \cup \{E_4\}$ which is the boundary of two basins of attraction $\mathcal{B}(\mathbf{0})$ and $\mathcal{B}(E_5)$;

  (iii) on HL curve between regions **III** and **V** homoclinic loop Γ at a saddle E_4 surround a stable limit cycle γ_1, creating an unstable separatrix cycle $\Gamma^- = \Gamma \cup \{E_4\}$ which is the boundary of two basins of attraction $\mathcal{B}(\mathbf{0})$ and $\mathcal{B}(\gamma_1)$.

For a bifurcation diagram on Figure 13, in addition to all the above conclusions, the system shows another specific dynamic. On H curve two more GH points appears. Moving anticlockwise at H curve from BT_1 to BT_2 we have three GH points, denoted one after the other by GH_1, GH_2 and GH_3. Therefore, on H curve, Hopf bifurcation is subcritical between BT_1 point and GH_1 point, supercritical between GH_1 and GH_2 points, again subcritical between GH_2 and GH_3 points, and finally again supercritical between GH_3 point and BT_2 point. So, multiple changes of the number and the stability of limit cycles is observed. One more small parametric region **VII** is produced in which the model exhibits two limit cycles, but in this case one limit cycle is unstable surrounding stable interior equilibrium, while another is a stable one surrounding

the unstable limit cycle. This results in a multiple coexistence of predator and prey, with either a stable oscillations of both populations or with a stable periodic coexistence, for all initial values lying inside the unstable limit cycle.

Considering the obtained bifurcation diagrams (See Figures 11,13 and 14), we can see that, as value of parameter a decreases, range of parameter m for which coexistence is possible expands. More specifically, the only regions where populations will always go extinct are regions **I** and **II**. To ensure populations have a chance at surviving, we must control the values of parameters a and m, which can be done in several ways. By increasing the intrinsic growth rate of prey r or its carrying capacity K, values of parameters a and m will decrease. Coexistence can be guaranteed also by increasing the effectiveness of predator's hunts, namely by increasing the attack rate e and the amount of prey killed with each encounter C. With these changes, only the value of parameter a gets decreased. While it may seem paradoxical, it is important to note that for SAE, growth rate of prey population is largest precisely for population densities that are slightly larger than the threshold. This way, even with larger predator population and with regular hunts, prey population can compensate for the suffered losses made by predator hunting and both population will persist.

Multiple attractors:

(a) Bifurcation analysis shows that our ecological model (9) in the case of SAE generates multiple attractors in a small parametric region. One of them is always the origin, so that model may exhibits bi-stability either between the origin and a stable interior equilibrium points or between the origin and a stable limit cycle. Thus, for the same set of parameter values, both populations can coexist oscillating around specific population sizes or both species will be extinct. Also, stable periodic coexistence or extinction of both species is possible for the same set of parameter values. Moreover, our model may even exhibits tri-stability in the case that stable interior equilibrium is surrounded by two limit cycles wherby the stable limit cycle encloses an unstable limit cycle. Therefore, strong Allee effect causes the models to be sensitive to initial conditions. All coexistence scenarios were considered and basins of attraction of multiple attractors are determined by the relative positions of stable and unstable manifolds of saddle points E_2, E_4 and unstable node E_2, which may change under perturbation.

Considering the obtained basins (see Figures 16,18,19), we can deduce that, in the case of SAE, populations will coexist only when predator population is not too numbered. This only confirms the statement Cosner made in [8] which states that when the number of predators is too high, the forage line is too long for efficient hunting. This will lead to the reduced predator population, but not before prey population becomes too low to allow coexistence. In certain cases, quantity of prey population also limits coexistence. If prey population is too numbered, coexistence will be impossible to achieve due to overexploitation by prey population. It is also clear that parameters tied to predator population and its characteristics also affect the behaviour of the system. However, exact reason can not be inferred.

(b) In the case of WAE, total extinction of the population is never possible since the origin is a local repeller. Model may only exhibits multiple stable coexistence, so that for the same values of parameters populations will coexist either with a stable periodic or with a oscillatory periodic behavior, depending on the initial value. Through generalized Hopf bifurcation unstable limit cycle create the boundary of the basin of attraction of the stable equilibrium point and a stable limit cycle.

Comparing the model (9) with predator-prey model (4) without Allee effects considered in [22], it is observed that a strong Allee effect significantly modifies the original system dynamics. The system (4) has a predator-free equilibrium which is a saddle point and a unique interior equilibrium that can be globally stable for certain parameter values. Also, system (4) undergoes supercritical Hopf bifurcation and supercritical generalized Hopf bifurcation at non-hyperbolic interior equilibrium. Therefore, weak Allee effect does not change significantly dynamic behavior of the model (4), since there is a wide range of initial values that allow the two populations to coexist and both model demonstrates the existence of a bi-stability phenomenon. However, the strong Allee effect drive the model (9) to the possibility of total extinction. Thus, although bi-stability is observed in both models, implying that models are highly sensitive to the initial conditions, in the model without Allee effect bi-stability is reflected in different forms of coexistence of predator and prey, while in the model with a strong Allee effect bi-stability effect is critical and different initial conditions lead to the extinction of both species or to coexistence. Moreover, we have shown that the

bifurcation structure is richer than when the strong Allee effect is absent.

In order to conclude how the increasing functional response (3) changes the dynamics of the Leslie–Gower mathematical model with the Holling type II and IV function responses, we compare the system (9) with systems (6) and (7). Systems (9) and (6) with strong Allee effect exhibit qualitatively similar dynamics. Both systems always have two unstable axial equilibria, the number of interior equilibria vary from zero to two and in the case of the existence of two interior equilibria one is always a saddle, while the other can be an attract or a repeller. Both systems can undergo Bogdanov-Takens bifurcation of codimension 2 and has a limit cycle or homoclinic loop. Also, the origin is an local attractor and both populations may coexist at some stable interior equilibria. The dynamics of both models demonstrate the existence of bi-stability phenomenon. Since the origin is always an attractor, we have that different conditions lead to the extinction of both species or to coexistence of predator and prey populations at some stable interior equilibria. However, fundamental difference is reflected in stability and number of limit cycles, leading to stable oscillatory coexistence of predator and prey as well as to multiple stable coexistence. In fact, unlike system (6) where the limit cycle cannot be an attractor, in system (9) we observe not only the existence of a stable limit cycle, but also the existence of both supercritical and subcritical generalized Hopf bifurcation, through which the interior equilibrium point can be surrounded by two limit cycles, one of which is always an attractor. Thus, system (9) as opposed system (6) can have at most three attractors in the first quadrant. Therefore, the increasing functional response presented in this manuscript changes the dynamics of the systems with the Holling type II function response, since the limit cycles have different stability, implying different coexistence behavior.

Comparing the model (9) with the Leslie–Gower type model (7) with Holling type IV functional response, it is observed that both systems undergoes various kinds of bifurcations at non-hyperbolic interior equilibria, such as saddle–node bifurcation, Hopf bifurcation, degenerate Hopf bifurcation and BT bifurcation of codimensions 2. However, model (7) admits one *GH* and one *BT* codimensions two bifurcation points, while model (9) generates two *BT* codimension two bifurcation points and for certain parameter values it may generate three *GH* bifurcation points. Although the bi-stability, basins of attraction of multiple attractors and extinction conditions were not been explicitly considered in [24], model (7) shows bi-stability behavior, that is prey and predator will be extinct or oscillate periodically depending on the initial value. On the other hand, in our model, multiple changes of the stability of limit cycles results not only in a bi-stable phenomenon, but also a tri-stable phenomenon and the multiple coexistence of species is possible. Therefore, the increasing functional response enhances and modifies the dynamics of the model with Holling type IV functional response.

7. Appendix

7.1. Appendix A.1. Proof of Theorem 3.3

By translating equilibrium E_{bt} to the origin with the transformations $X = x - x_{bt}, Y = y - y_{bt}$, system (9) can be rewritten as:

$$\dot{X} = a_{10}X + a_{01}Y + a_{20}X^2 + a_{11}XY + a_{02}Y^2 + O(|X, Y|^3)$$
$$\dot{Y} = b_{10}X + b_{01}Y + b_{20}X^2 + b_{11}XY + b_{02}Y^2 + O(|X, Y|^3),$$

where:

$$a_{10} = b, \quad a_{01} = -c, \quad a_{20} = 1 + m_{bt} - 3x_{bt} + \frac{a_{bt}b^3 x_{bt}^3}{(c + bx_{bt}^2)^3}, \quad a_{11} = -\frac{2a_{bt}bc^2 x_{bt}}{(c + bx_{bt}^2)^3}, \quad a_{02} = -\frac{ac^3 x_{bt}}{(c + bx_{bt}^2)^3},$$

$$b_{10} = \frac{b^2}{c}, \quad b_{01} = -b, \quad b_{20} = -\frac{b^2}{cx_{bt}}, \quad b_{11} = \frac{2b}{x_{bt}}, \quad b_{02} = -\frac{c}{x_{bt}}.$$

The linear part of this system can be transformed into Jordan canonical form by using the following transformation:

$$X = \frac{c}{b}x_1 + \frac{c}{b^2}y_1, \quad Y = x_1.$$

The obtained system is

$$\dot{x}_1 = y_1 + c_{20}x_1^2 + c_{11}x_1y_1 + c_{02}y_1^2 + O(|x_1, x_2|^3)$$
$$\dot{y}_1 = d_{20}x_1^2 + d_{11}x_1y_1 + d_{02}y_1^2 + O(|x_1, x_2|^3),$$

where:

$$c_{20} = \frac{b_{20}b_{01}^2}{b_{10}^2} - \frac{b_{11}b_{01}}{b_{10}} + b_{02}, \quad c_{11} = \frac{b_{11}}{b_{10}} - \frac{2b_{20}b_{01}}{b_{10}^2}, \quad d_{11} = \frac{a_{11}b_{10}^2 - 2a_{20}b_{01}b_{10} - 2b_{01}^2b_{10} + b_{01}b_{10}b_{11}}{b_{10}^2},$$

$$d_{20} = \frac{a_{02}b_{10}^3 - a_{11}b_{01}b_{10}^2 + a_{20}b_{01}^2b_{10} + b_{01}^3b_{20} - b_{01}^2b_{10}b_{11} + b_{01}b_{02}b_{10}^2}{b_{10}^2}, \quad c_{02} = \frac{b_{20}}{b_{11}^2}, \quad d_{02} = \frac{a_{20}b_{10} + b_{01}b_{20}}{b_{10}^2}.$$

Further, with the change of coordinates

$$x_1 = x_2 + \frac{c_{11} + d_{02}}{2}x_2^2, \quad y_1 = y_2 - c_{20}x_2^2 + d_{20}x_2y_2 - c_{02}y_2^2,$$

we obtain the following system:

$$\dot{x}_2 = y_2 + O(|x_2, y_2|^3)$$
$$\dot{y}_2 = s_1x_2^2 + s_2x_2y_2 + O(|x_2, y_2|^3),$$

where s_1 and s_2 are given with (26). By the results in [19], the origin is a cusp of codimension 2 if $s_1s_2 \neq 0$. It follows that interior equilibrium $E_{bt}(x_{bt}, y_{bt})$ of system (9) is Bogdanov-Takens singularity under the same assumption. This concludes the proof of the theorem.

7.2. Appendix A.2. Transversality of Bogdanov-Takens (BT) bifurcation

To show that system (9) undergoes the Bogdanov-Takens bifurcation when (a, m) varies in the neighborhood of (a_{bt}, m_{bt}), we consider the following unfolding of the system (9)

$$\dot{x} = x(1 - x)(x - (m_{bt} + \varepsilon_1)) - \frac{(a_{bt} + \varepsilon_2)xy^2}{1 + xy}$$
$$\dot{y} = by - c\frac{y^2}{x}. \tag{27}$$

where ε_1 and ε_2 are small parameters varying in the small neighborhood of the origin. Next, we reduce the system (27) in the normal form of a Bogdanov-Takens bifurcation, by employing a series of change of coordinates in a small neighborhood of the origin. First, translating the equilibrium $E_{bt}(x_{bt}, y_{bt})$ to the origin with $X = x - x_{bt}, Y = y - y_{bt}$, the power series of the obtained system is given by:

$$\dot{X} = g_{00} + g_{10}X + g_{01}Y + g_{20}X^2 + g_{11}XY + g_{02}Y^2 + O(|X, Y|^3)$$
$$\dot{Y} = h_{10}X + h_{01}Y + h_{20}X^2 + h_{11}XY + h_{02}Y^2 + O(|X, Y|^3). \tag{28}$$

Coefficients of the system (28) are found in Appendix A.3 and the coefficients depend smoothly on $\varepsilon = (\varepsilon_1, \varepsilon_2)$. Given that $g_{01}g_{02} \neq 0$ for small values of ε, system (28) can be further transformed by using the change of variable:

$$x_1 = X, \quad y_1 = g_{00} + g_{10}X + g_{01}Y + g_{20}X^2 + g_{11}XY + g_{02}Y^2 + O(|X, Y|^3).$$

We obtain

$$\dot{x}_1 = y_1$$
$$\dot{y}_1 = s_{00} + s_{10}x_1 + s_{01}y_1 + s_{20}x_1^2 + s_{11}x_1y_1 + s_{02}y_1^2 + O(|x_1, y_1|^3). \tag{29}$$

where all coefficient are given in Appendix A.4. and the coefficients depend smoothly on ε. Further, we make a time scale transformation $dt = (1 - s_{02}x_1)d\tau$ and obtain

$$\frac{dx_1}{d\tau} = y_1 - s_{02}x_1y_1$$

$$\frac{dy_1}{d\tau} = s_{00} + (s_{10} - s_{00}s_{02})x_1 + s_{01}y_1 + (s_{20} - s_{10}s_{02})x_1^2 + (s_{11} - s_{01}s_{02})x_1y_1 + s_{02}y_1^2 + O(|x_1, y_1|^3). \tag{30}$$

Direction of time is preserved near the origin. Then, with a coordinate transformation: $x_2 = x_1$, $y_2 = y_1 - s_{02}x_1y_1$, the system (30) becomes

$$\frac{dx_2}{d\tau} = y_2$$

$$\frac{dy_2}{d\tau} = r_{00} + r_{10}x_2 + r_{01}y_2 + r_{20}x_2^2 + r_{11}x_2y_2 + O(|x_2, y_2|^3). \tag{31}$$

Coefficients of the system (31) are found in Appendix A.5. and the coefficients depend smoothly on ε. Note that for $\varepsilon_1 = \varepsilon_2 = 0$, we have: $r_{20} = cs_1/b$, $r_{11} = cs_2/b$, where s_1 and s_2 are given with (26). Given that condition $s_1s_2 \neq 0$ must hold for E_{bt} to be cusp point, we deduce that $r_{20}r_{11} \neq 0$, when $\varepsilon_1 = \varepsilon_2 = 0$. To eliminate term y_2 in the system (31), we make the change of variable:

$$x_3 = x_2 + \frac{r_{01}}{r_{11}}, \quad y_3 = y_2.$$

Thus, we obtain the system:

$$\frac{dx_3}{d\tau} = y_3$$

$$\frac{dy_3}{d\tau} = C_1 + C_2x_3 + r_{20}x_3^2 + r_{11}x_3y_3 + O(|x_3, y_3|^3). \tag{32}$$

Coefficients of the system (32) are found in Appendix A.6. and the coefficients depend smoothly on ε. By introducing new time variable $\tau = \left|\frac{r_{11}}{r_{20}}\right| s$, and introducing the change of variables again:

$$\overline{x} = \frac{r_{20}}{r_{11}^2}x_3, \quad \overline{y} = \text{sign}\left(\frac{r_{11}}{r_{20}}\right)\frac{r_{20}^2}{r_{11}^3}y_3,$$

after dropping the bars and denoting s with t, the system (32) obtains the form which is a normal form of BT bifurcation

$$\frac{dx}{dt} = y$$

$$\frac{dy}{dt} = \mu_1 + \mu_2 x + x^2 + S xy + O(|x, y|^3), \tag{33}$$

where

$$\mu_1 = \frac{r_{11}^4}{r_{20}^3}C_1, \quad \mu_2 = \frac{r_{11}^2}{r_{20}^2}C_2, \quad S = \text{sign}\frac{r_{11}}{r_{20}}\Big|_{\varepsilon_1=0,\varepsilon_2=0}.$$

Observe the map $(x, y, \varepsilon_1, \varepsilon_2) \rightarrow (f(x, y, \varepsilon_1, \varepsilon_2), tr(J(x, y)), det(J(x, y)))$, where $f(x, y, \varepsilon_1, \varepsilon_2) = (f_1(x, y, \varepsilon_1, \varepsilon_2), f_2(x, y, \varepsilon_1, \varepsilon_2))$ is a vector field of the system (28) and $J(x, y) = \frac{\partial(f_1, f_2)}{\partial(x,y)}$. The transversality condition for Bogdanov-Takens bifurcation is equivalent to the regularity of this map at $(0, 0, 0, 0)$, which is satisfied if:

$$\frac{D(f, tr(J), det(J))}{D(x, y, \varepsilon_1, \varepsilon_2)} = \frac{b^4 x_{bt}}{c(c + bx_{bt}^2)^2(2c + bx_{bt}^2)}\Big(b^3 x_{bt}^5(2x_{bt} - 1) + 4c^2 x_{bt}(1 - 4x_{bt} + 7x_{bt}^2 - 4x_{bt}^3)$$

$$+ b^2\Big(x_{bt}^5 - 4x_{bt}^6 + 7x_{bt}^7 - 4x_{bt}^8 + cx_{bt}^2(-2 - 3x_{bt} + 8x_{bt}^2)\Big)$$

$$- 2bc\Big(c(2 - 3x_{bt} + 2x_{bt}^2) + 2x_{bt}^3(-1 + 4x_{bt} - 7x_{bt}^2 + 4x_{bt}^3)\Big)\Big) \neq 0.$$

According to the results in [14], system (33) (i.e. (28)), undergoes either repelling or attracting Bogdanov-Takens bifurcation around E_{bt} as parameters (a, m) vary in the small neighborhood of (a_{bt}, m_{bt}), depending on S in (33), and it is concluded:

(i) If $S > 0$, system undergoes supercritical Bogdanov-Takens bifurcation, which includes a sequence of bifurcations of codimension 1: saddle-node bifurcation, supercritical Hopf bifurcation and homoclinic bifurcation

(ii) If $S < 0$, system undergoes subcritical. Bogdanov-Takens bifurcation, which includes a sequence of bifurcations of codimension 1: saddle-node bifurcation, subcritical Hopf bifurcation and homoclinic bifurcation.

Analytical expressions for μ_1 and μ_2 in terms of ε_1 and ε_2 are difficult to obtain. Therefore, local representations of bifurcation curves are given by:

- Saddle-node bifurcation curve: $SN = \{(\varepsilon_1, \varepsilon_2) : 4\mu_1(\varepsilon_1, \varepsilon_2) - \mu_2^2(\varepsilon_1, \varepsilon_2) = 0\}$.

- Hopf bifurcation curve: $H = \{(\varepsilon_1, \varepsilon_2) : \mu_1(\varepsilon_1, \varepsilon_2) = 0, \quad \mu_2(\varepsilon_1, \varepsilon_2) < 0\}$.

- Homoclinic bifurcation curve: $HL = \{(\varepsilon_1, \varepsilon_2) : 25\mu_1(\varepsilon_1, \varepsilon_2) + 6\mu_2^2(\varepsilon_1, \varepsilon_2) = 0, \quad \mu_2(\varepsilon_1, \varepsilon_2) < 0\}$.

7.3. Appendix A.3.

Coefficients of the system (28):

$$g_{00} = \varepsilon_1(x_{bt} - 1)x_{bt} - \frac{b^2\varepsilon_2 x_{bt}^3}{c(c + bx_{bt}^2)}, \quad g_{01} = -\frac{b(a + \varepsilon_2)x_{bt}^2(2c + bx_{bt}^2)}{(c + bx_{bt}^2)^2}, \quad g_{02} = -\frac{c^2(a + \varepsilon_2)x_{bt}}{(c + bx_{bt}^2)^3},$$

$$g_{10} = (\varepsilon_1 + m)(2x_{bt} - 1) + x_{bt}\left(2 - 3x_{bt} - \frac{b^2(a + \varepsilon_2)x_{bt}}{(c + bx_{bt}^2)^2}\right), \quad g_{11} = -\frac{2bc^2(a + \varepsilon_2)x_{bt}}{(c + bx_{bt}^2)^3},$$

$$g_{20} = 1 + \varepsilon_1 + m - 3x_{bt} + \frac{b^3(a + \varepsilon_2)x_{bt}^3}{(c + bx_{bt}^2)^3}, \quad h_{10} = \frac{b^2}{c}, \quad h_{01} = -b, \quad h_{20} = -\frac{b^2}{cx_{bt}}, \quad h_{11} = \frac{2b}{x_{bt}}, \quad h_{02} = -\frac{c}{x_{bt}}.$$

7.4. Appendix A.4.

Coefficients of the system (29):

$$s_{00} = -g_{00}h_{01} + \frac{g_{01}^3 h_{02}}{2g_{02}^2} + \frac{g_{00}^2(g_{02}h_{01} + g_{01}h_{02})}{g_{01}^2},$$

$$s_{01} = -\frac{g_{00}g_{02}(g_{00}g_{01}g_{11} + 2g_{01}^2 h_{01} + 6g_{00}g_{02}h_{01}) - g_{01}^4(g_{10} + h_{01}) + g_{00}g_{01}^3(g_{11} + 2h_{02})}{g_{01}^4},$$

$$s_{10} = \left(\frac{2g_{00}g_{02}(g_{01}^2 + 3g_{00}g_{02})}{g_{01}^4} - 1\right)g_{10}h_{01} + \frac{2g_{00}g_{10}h_{02}}{g_{01}} + g_{01}h_{10} + \frac{g_{00}(2g_{02}h_{10} + g_{01}h_{11})}{g_{01}}$$

$$+ \frac{g_{00}^2(-2g_{02}g_{11}h_{01} - g_{01}g_{11}h_{02} - 2g_{02}^2 h_{10} + g_{01}g_{02}h_{11})}{g_{01}^3},$$

$$
\begin{aligned}
s_{20} = & -g_{20}h_{01} + g_{11}h_{10} - g_{10}h_{11} + g_{01}h_{20} + \frac{3g_{00}g_{02}\big(g_{00}g_{11}^2 h_{01} + 2g_{02}(g_{10}^2 h_{01} + g_{00}(g_{20}h_{01} + g_{11}h_{10} + g_{10}h_{11}))\big)}{g_{01}^4} \\
& - \frac{6g_{00}^2 g_{02}^2 g_{10}(4g_{11}h_{01} + g_{10}h_{02})}{g_{01}^5} + \frac{g_{10}^2 h_{02} + 2g_{00}g_{20}h_{02} - 2g_{02}g_{10}h_{10} - 2g_{00}g_{02}h_{20}}{g_{01}} \\
& + \frac{-2g_{00}g_{10}g_{11}h_{02} + g_{02}(g_{10}^2 h_{01} + 2g_{00}(g_{20}h_{01} + g_{11}h_{10} + g_{10}h_{11}))}{g_{01}^2} \\
& - \frac{g_{00}(-g_{00}g_{11}^2 h_{02} + 2g_{02}g_{11}(2g_{10}h_{01} + g_{00}h_{11}) + 2g_{02}^2(2g_{10}h_{10} + g_{00}h_{20}))}{g_{01}^3}, \\
s_{11} = & \frac{1}{g_{01}^5}\Big(6g_{00}^2 g_{02}^2(-g_{10}g_{11} + 4g_{11}h_{01} + 2g_{10}h_{02}) - g_{01}^4(g_{10}(g_{11} + 2h_{02}) - 2g_{02}h_{10}) \\
& + 2g_{00}g_{01}^2 g_{02}(-g_{10}g_{11} + 2g_{11}h_{01} + 2g_{02}h_{10}) + g_{01}^5(2g_{20} + h_{11}) \\
& + 3g_{00}g_{01}g_{02}(-4g_{02}g_{10}h_{01} + g_{00}(a_{11}^2 - 2g_{02}h_{11})) + g_{01}^3(-2g_{02}g_{10}h_{01} + g_{00}(g_{11}^2 + 2g_{11}h_{02} - 2g_{02}h_{11}))\Big), \\
s_{02} = & \frac{g_{01}g_{02}(2g_{00}g_{01}g_{11} + g_{01}^2 h_{01} + 6g_{00}g_{02}h_{01}) + 6g_{00}^2 g_{02}^2(g_{11} - h_{02}) + g_{01}^4(g_{11} + h_{02})}{g_{01}^5}.
\end{aligned}
$$

7.5. Appendix A.5.

Coefficients of the system (31):

$$
r_{00} = s_{00}, \quad r_{10} = -2s_{00}s_{02} + s_{10}, \quad r_{01} = s_{01}, \quad r_{20} = s_{00}s_{02}^2 - 2s_{02}s_{10} + s_{20}, \quad r_{11} = -s_{01}s_{02} + s_{11}.
$$

7.6. Appendix A.6.

Coefficients of the system (32):

$$
C_1 = r_{00} + \frac{r_{01}(-r_{10}r_{11} + r_{01}r_{20})}{r_{11}^2}, \quad C_2 = r_{10} - \frac{2r_{01}r_{20}}{r_{11}}.
$$

References

[1] W.C. Allee, *Animal Aggregations: A Study in General Sociology*, University of Chicago Press, Chicago (1931).
[2] M.T. Alves, F.M. Hilker, *Hunting cooperation and Allee effects in predators*. J. Theoret. Biol. **419** (2017), pp. 13–22.
[3] C. Arancibia-Ibarra, J.D. Flores, G. Petter, P. Heijster, *A Holling–Tanner Predator–Prey Model with Strong Allee Effect*, Internat. J. Bifur. Chaos Appl. Sci. Engrg. **29** (2019), No. 11, 1930032, (16) pages.
[4] L. Berec, *Impacts of foraging facilitation among predators on predator-prey dynamics*. Bull. Math. Biol **72** (2010), pp. 94–121.
[5] L. Berec, E. Angulo, F. Courchamp, *Multiple Allee effects and population management*, Trends Ecol. Evol. **22** (2007), No. 4, pp. 185–191.
[6] R. Bogdanov, *Bifurcations of a limit cycle for a family of vector fields on the plane*, Sel. Math. Sov. **1** (1981), No. 4, pp. 373–388.
[7] R. Bogdanov, *Versal deformations of a singular point on the plane in the case of zero eigen-values*, Sel. Math. Sov. **1** (1981), No. 4, pp. 389–421.
[8] C. Cosner, D.L. Deangelis, J.S. Ault, D.B. Olson, *Effects of Spatial Grouping on the Functional Response of Predators*, Theor. Popul. Biol. **56** (1999), No. 1, pp. 65 − 75.
[9] F. Courchamp, L. Berec, J. Gascoigne, *Allee effects in Ecology and Conservation*, Oxford University Press, Oxford, (2008).
[10] A. Dhooge, W. Govaerts, Yu. A. Kuznetsov, *MATCONT: A MATLAB package for numerical bifurcation analysis of ODEs*, ACM Trans. Math. Software **29** (2003), No. 2, pp. 141–164.
[11] F. Dumortier, J. Llibre, J. C. Artés, Qualitative Theory of Planar Differential Systems, Springer-Verlag, Berlin, Heidelberg, (2006).
[12] R. P. Gupta, P. Chandra, *Bifurcation analysis of modified Leslie–Gower predator–prey model with Michaelis–Menten type prey harvesting*, J. Math. Anal. Appl. **398** (2013), No. 1, pp. 278 − 295.
[13] R. E. Kooij, A. Zegeling, *A Predator-Prey Model with Ivlev's Functional Response*, J. Math. Anal. Appl. **198** (1996), No. 2, pp. 473 − 489.
[14] Yu. A. Kuznetsov, *Elements of Applied Bifurcation Theory* , Springer-Verlag, Berlin, Heidelberg, (2004).
[15] Z. Lajmiri, R. Khoshsiar Ghaziani, I. Orak, *Bifurcation and stability analysis of a ratio-dependent predator-prey model with predator harvesting rate*, Chaos Solitons Fractals **106** (2018), pp. 193 − 200.
[16] Y. Lamontagne, C.Coutu, C. Rousseau, *Bifurcation Analysis of a Predator–Prey System with Generalised Holling Type III Functional Response*, J. Dynam. Differential Equations **20** (2008), No. 3, pp. 535 − 571.

[17] P. H. Leslie, J.C. Gower, *The properties of a stochastic model for the predator-prey type of interaction between two species*, Biometrika **47** (1960), No. 3 − 4, pp. 219–34.

[18] P. S. Mandal, U. Kumar, K. Garain, R. Sharma, *Allee effect can simplify the dynamics of a prey-predator model*, J. Appl. Math. Comput. **63** (2020), No. 1 − 2, pp. 739 − 770.

[19] L. Perko, *Differential Equations and Dynamical Systems*, Springer-Verlag, New York, (2001).

[20] A. Rojas-Palma, E. González-Olivares, *Optimal harvesting in a predator–prey model with Allee effect and sigmoid functional response*, Appl. Math. Model. **36** (2012), No. 5, pp. 1864 − 1874.

[21] K. Ryu, W. Ko, M. Haque, *Bifurcation analysis in a predator–prey system with a functional response increasing in both predator and prey densities*, Nonlinear Dynamics **94** (2018), No. 1, pp. 1639 − 1656.

[22] Z. Shang, Y. Qiao, L. Duan, J. Miao, *Bifurcation analysis and global dynamics in a predator–prey system of Leslie type with an increasing functional response*, Ecological Modelling **455** (2021), 109660, (12) pages.

[23] Z. Shang, Y. Qiao, L. Duan, J. Miao, *Bifurcation analysis in a predator–prey system with an increasing functional response and constant-yield prey harvesting*, Math. Comput. Simulation **190** (2021), pp. 976 − 1002.

[24] Z. Shang, Y. Qiao, *Bifurcation analysis of a Leslie-type predator–prey system with simplified Holling type IV functional response and strong Allee effect on prey*, Nonlinear Analysis: Real World Applications **64** (2022), 103453, (34) pages.

[25] P.A. Stephens, W.J. Sutherland, *Consequences of the Allee effect for behaviour, ecology and conservation*, Trends Ecol. Evol. **14** (1999), No. 10, pp. 401–405.

[26] F. Takens, *Forced oscillations and bifurcation*, Applications of Global Analysis I, Comm. Math. Inst. Rijksuniversitat Utrecht. **3** (1974), pp. 1–59.

[27] B. Tiwari, S. N. Raw, *Qualitative analysis of a spatiotemporal prey–predator model with multiple Allee effect and schooling behaviour*, Nonlinear Dynamics **102** (2020), No. 10, pp. 3013 − 3038.

[28] P. Turchin, *Complex Population Dynamics. A Theoretical/Empirical Synthesis*, Monographs in Population Biology **35** (2003), Princeton University Press.

[29] L. Wu, H. Zheng, S. Zhang, *Dynamics of a non-autonomous predator-prey system with Hassell-Varley-Holling II function response and mutual interference*, AIMS Math. **6** (2021), No. 6, pp. 6033 − 6049.

[30] P. Ye, D. Wu, *Impacts of strong Allee effect and hunting cooperation for a Leslie-Gower predator-prey system*, Chinese J. Phys. **68** (2020), No. 1, pp. 49 − 64.

[31] Y. Ye, H. Liu, Y.Wei, K. Zhang, M. Ma, J. Ye, *Dynamic study of a predator-prey model with Allee effect and Holling type-I functional response*, Advances in Difference Equations **1** (2019), No. 369, (15) pages.

[32] Y. Zhang, J. Huang, *Bifurcation analysis of a predator-prey model with Beddington–DeAngelis functional response and predator competition*, Math. Methods Appl. Sci. **45** (2022), No. 16, pp. 9894 − 9927,

[33] H. Zhu, S. A. Campbell, G. S. K. Wolkowicz, *Bifurcation Analysis of a Predator-prey System with Nonmonotonic Functional Response*, §SIAM J. Appl. Math. **63** (2003), No. 2, pp. 636 − 682.